The Southern 2MASS Active Galactic Nuclei Survey: Spectroscopic Follow-up with Six Degree Field

Frank J. Masci[A,E], *Roc M. Cutri*[A], *Paul J. Francis*[B], *Brant O. Nelson*[A,F], *John P. Huchra*[C], *D. Heath Jones*[D], *Matthew Colless*[D], *and Will Saunders*[D]

[A] Infrared Processing and Analysis Center, Caltech 100-22, Pasadena, CA 91125, USA
[B] Australian National University, ACT 0200, Australia
[C] Harvard-Smithsonian Center for Astrophysics, Cambridge, MA 02138, USA
[D] Anglo-Australian Observatory, PO Box 296, Epping, NSW 1710, Australia
[E] Corresponding author. Email: fmasci@caltech.edu
[F] Present address: Vermont Academy, Saxtons River, VT 05154, USA

Abstract: The Two Micron All-Sky Survey (2MASS) has provided a uniform photometric catalog to search for previously unknown red active galactic nuclei (AGN) and Quasi-Stellar Objects (QSOs). We have extended the search to the southern equatorial sky by obtaining spectra for 1182 AGN candidates using the six degree field (6dF) multifibre spectrograph on the UK Schmidt Telescope. These were scheduled as auxiliary targets for the 6dF Galaxy Redshift Survey. The candidates were selected using a single color cut of $J - K_s > 2$ to $K_s \lesssim 15.5$ and a galactic latitude of $|b| > 30°$. 432 spectra were of sufficient quality to enable a reliable classification. 116 sources ($\sim$27%) were securely classified as type I AGN, 20 as probable type I AGN, and 57 as probable type II AGN. Most of them span the redshift range $0.05 < z < 0.5$ and only 8 ($\sim$6%) were previously identified as AGN or QSOs. Our selection leads to a significantly higher AGN identification rate amongst local galaxies ($>$20%) than in any previous (mostly blue-selected) galaxy survey. A small fraction of the type I AGN could have their optical colors reddened by optically thin dust with $A_V < 2$ mag relative to optically selected QSOs. A handful show evidence of excess far-infrared (IR) emission. The equivalent width (EW) and color distributions of the type I and II AGN are consistent with AGN unified models. In particular, the EW of the [OIII] emission line weakly correlates with optical–near-IR color in each class of AGN, suggesting anisotropic obscuration of the AGN continuum. Overall, the optical properties of the 2MASS red AGN are not dramatically different from those of optically-selected QSOs. Our near-IR selection appears to detect the most near-IR luminous QSOs in the local universe to $z \simeq 0.6$ and provides incentive to extend the search to deeper near-IR surveys.

Keywords: galaxies: active — quasars: general — infrared: general — surveys

1 Introduction

Much of our knowledge about the distribution and properties of active galactic nuclei (AGN) has come from samples that are flux-limited at blue optical wavelengths. This is because their spectral energy distributions (SEDs) generally exhibit a UV flux excess. Such surveys can be very efficient and complete down to their blue flux limit, e.g., the Large Bright Quasar Survey (LBQS; Hewett et al. 1995). However, any survey with a blue flux limit will be relatively biased against objects whose intrinsic emission peaks at other wavelengths, e.g., near-infrared (IR) emission from the host galaxy (Masci et al. 1998; Benn et al. 1998). Alternatively, the optical/UV can be partially or heavily absorbed by dust, as revealed by radio, near-to-mid IR, and X-ray surveys (Webster et al. 1995; Gregg et al. 2002; Polletta et al. 2007; Donley et al. 2008). The Sloan Digital Sky Survey (SDSS; Richards et al.

2002) has employed a range of multicolor optical selection techniques with relaxed constraints on morphology to search for QSOs to redshifts of $\simeq$6. This has reduced the bias relative to the simple UV-excess criteria used in early surveys, but has not eliminated it.

A complete census of AGN over cosmic time is essential for understanding galaxy formation and evolution since the properties of the central black hole and host galaxy are intimately linked (see reviews in Ho 2004). The fraction of AGN missing from optically selected samples, both as a function of redshift and luminosity, is an important parameter. This is expected to be related to the duty cycle of black-hole fueling and timescales for regulating star formation. Values are currently very uncertain and range from 15% to greater than 50% (e.g., Richards et al. 2003; Glikman et al. 2004, 2007; Brown et al. 2006). This uncertainty is due to: selection of the appropriate

comparison sample of optically selected AGN; properties of the 'unbiased' sample and how representative it is; and difficulties in quantifying the amount of bias (e.g., dust extinction).

1.1 Near-IR Selection

Warren et al. (2000) showed that it is possible to construct a complete K-band–limited QSO sample by combining optical and near-IR photometry. This exploits the characteristic K-band excess seen in QSOs compared to stars and has been termed the KX-selection method. A number of small pilot surveys have employed KX-selection and variants thereof (e.g., Croom et al. 2001; Sharp et al. 2002; Jurek et al. 2008; Smail et al. 2008). The largest is being compiled from the UKIDSS Large Area Survey covering $\sim 12.8\,\mathrm{deg}^2$ (Maddox et al. 2008). This survey currently reports a surface density of $\simeq 15\,\mathrm{deg}^{-2}$ for broad-lined AGN with $K \leq 17$ and $z < 3$. They estimated that $\sim 50\%$ were missed by SDSS, therefore revealing a large population of red QSOs.

Although the KX method is turning up many luminous red QSOs to high redshift, the situation is different for less luminous local AGN (e.g., Seyfert nuclei). These are usually not found by color selection since host galaxy light can dominate their broadband colors. Historically, they are found by taking optical spectra of the nuclear regions of large samples of galaxies (e.g., Ho et al. 1997). Many of these samples are flux-limited at blue optical wavelengths and hence subject to bias. The most significant bias is that the blue light is dominated by recent star formation which overwhelms any emission from a central AGN. A near-IR selected sample of local galaxies using color criteria analogous to that used in KX methods will reduce this bias.

The largest near-IR survey to date is the Two Micron All Sky Survey (2MASS; Skrutskie et al. 2006). There have been several studies that searched for AGN in 2MASS. The first was that from Cutri et al. (2002) in the northern equatorial sky. They selected sources with $J - K_s > 2$ and $K_s \leq 15.5$[1] at galactic latitude $|b| > 30°$. Spectroscopic follow-up revealed that $\sim 75\%$ were previously unidentified AGN, with $\sim 80\%$ of these associated with broad emission-line (type I) AGN — i.e., Seyfert 1s and QSOs — and the remainder were narrow-line (type II) AGN — typically Seyfert 2s, type II QSOs and liners. They spanned a redshift range of $0.03 < z < 2.52$ with a median of ~ 0.22, therefore, the AGN were predominately local. The extrapolated surface density of all AGN types was $\sim 0.57\,\mathrm{deg}^{-2}$, significantly higher than that of optically selected AGN at the same K_s magnitude. A significant fraction also showed unusually high polarization properties (Smith et al. 2002) and very weak X-ray emission (Wilkes et al. 2002).

Other 2MASS studies involved cross-correlating with the Faint Images of the Radio Sky at Twenty-centimeters

(FIRST) radio catalog (Gregg et al. 2002; Glikman et al. 2007). These revealed a number of extremely red QSOs at high redshift, some showing strong evidence for dust. Barkhouse & Hall (2001) studied the 2MASS colors of QSOs that were identified at other wavelengths, primarily from the Veron-Cetty & Veron (2000) catalog, and Georgakakis et al. (2009) used mid- and far-IR observations of red 2MASS AGN to infer their relationship to luminous IR galaxies (LIRGs). Most of these studies however used single band 2MASS detections (in J, H, or K_s) and therefore could have missed many red AGN. Furthermore, none were able to provide a census of AGN in the 2MASS catalog.

A uniform unbiased survey of 2MASS AGN was carried out by Francis et al. (2004) by selecting candidates in the southern hemisphere covering $12.56\,\mathrm{deg}^2$ using a moderate color cut of $J - K_s > 1.2$. This color cut significantly reduced contamination from foreground stars. Spectroscopic follow-up revealed that $\sim 1.2\%$ were broad-line AGN and $\sim 4\%$ were galaxies with Seyfert 2 nuclei. The main findings were that: (i) the type I AGN are predominately at low redshifts ($z \lesssim 0.3$) and contamination from host-galaxy light would make them hard to find in optically selected QSO samples (e.g., the SDSS); and (ii) the incidence of type II AGN amongst local galaxies is higher than usual when compared to blue-selected galaxy samples. The results of this study are complementary to those presented here and will be discussed in more detail later.

The above studies indicate that 2MASS is sensitive to the local AGN population. The luminosity of broad-lined QSOs, particularly in the local universe, is only slightly greater than that of their host galaxies (e.g., Hao & Strauss 2004). Only a small amount of dust extinction is needed to mis-identify them or turn them into type II AGN. This is in contrast to the heavily obscured, high-luminosity, and usually unresolved QSOs at high redshift. Therefore, even though near-IR color-selected surveys are less biased than those in the optical/UV, they are still somewhat biased against the reddest QSOs. They do however have the advantage that candidates selected in the near-IR will be bright enough to allow spectroscopic follow-up with relative ease.

It is worth mentioning why a red $J - K_s$ color cut has proven so efficient at finding AGN in the relatively shallow 2MASS Point Source Catalog (PSC). There are three reasons. First, contamination from halo-giant and disk-dwarf stars is very much eliminated, as the majority have $J - K_s \lesssim 0.75$ (Francis et al. 2004). Second, the 2MASS colors of galaxies are predominately blue, with a median $J - K_s \sim 1.1$ at $z \lesssim 0.1$ and a 1-σ upper limit of $J - K_s < 1.6$ at $z \simeq 0.2$ (Jarrett et al. 2000; Jarrett 2004). This color reddens rapidly for galaxies at higher redshifts due to the k-correction, approaching $J - K_s \simeq 2$ at $z \sim 0.4$. However, typical L^* galaxies at such redshifts will be well below the detection limit of the 2MASS PSC. Contamination from non-active galaxies is therefore expected to be small overall. The third reason is motivated by the fact

---

[1] K_s is similar to the K filter but cutting off at a shorter red wavelength to minimize thermal emission.

that an extremal color cut of $J - K_s > 2$ has been shown to discriminate red AGN from UV/optically-selected ones in large samples of known AGN (Barkhouse & Hall 2001; Cutri et al. 2002). For example, 2MASS detects a large fraction ($\sim$75%) of the LBQS QSOs in all three near-IR bands (J, H, and K_s). Most of these have $J - K_s < 2$. Therefore, $J - K_s > 2$ isolates the reddest subset of the optically selected population and is likely to probe many more. It is also interesting to note that nearly all known QSOs at $z \lesssim 0.5$ have $J - K_s > 1.2$ (Francis et al. 2000; Barkhouse & Hall 2001).

In this paper, we extend the work of Cutri et al. (2002) and Francis et al. (2004) to search for additional red 2MASS AGN in the southern equatorial sky. We assembled a relatively unbiased sample of red AGN candidates using a color cut of $J - K_s > 2$ on the 2MASS Point Source Working Database and then used the brute-force capabilities of the six degree field (6dF) multiobject spectrograph to obtain spectra of a subsample. We utlized the efficient mapping strategy of the 6dF Galaxy Survey (6dFGS) with our candidates selected as secondary targets in the program.

Our sample and target selection are described in Section 2. Observations and data reduction are described in Section 3, and spectral classifications in Section 4. Properties of the newly discovered AGN and comparisons to optically selected QSO samples are discussed in Section 5. Conclusions are given in Section 6. We assume a concordance cosmology with $H_0 = 70 \, \mathrm{km \, s^{-1} \, Mpc^{-1}}$, $\Omega_m = 0.3$, and $\Omega_\Lambda = 0.7$. All magnitudes, unless otherwise specified, are based on the Vega system.

2 Sample and Target Selection

Candidates were initially selected from the 2MASS Point Source Working Database using the following criteria: a color cut of $J - K_s > 2$; $K_s \leq 15.5$; detections in all three bands (J, H, and K_s); galactic latitude $|b| > 30°$; and excluding a region of $\sim$170 deg^2 covering the Large and Small Magellanic Clouds. Previously identified sources were not omitted. This yielded 16 977 candidates in an effective area of $\sim$20 400 deg^2 over the whole sky. These criteria define the 'master' catalog of red AGN candidates, and were used in northern hemisphere follow-up studies by Cutri et al. (2002).

Note that a detection in the H-band was included for reliability. The red AGN candidate selection criteria were originally devised during the early stages of the survey before many of the source quality metrics were mature. Sources detected in all three survey bands were known to be the most reliable. Therefore, three-band detection was included with the two-band color limit to minimize sample contamination by spurious sources with unusual colors.

Southern equatorial ($\delta < 0°$) AGN candidates from the master catalog were position matched against the Super-COSMOS Sky Survey database (Hambly et al. 2001a). A match radius of 4 arcsec was used and no optical

magnitude cut was initially imposed. Of matches, $\simeq$0.7% resulted in multiple (ambiguous) associations and were excluded. This yielded 6386 matches with an overall position-difference dispersion of $\sigma \simeq 0.6$ arcsec. A sample of 2260 candidates was then compiled by selecting sources with SuperCOSMOS magnitudes of $b_J \leq 18$ and $r_F \leq 17$. These limits were required to obtain good signal-to-noise ratio spectra ($S/N \gtrsim 10 \, \mathrm{pixel}^{-1}$) and enable reliable identifications. The reliability of the SuperCOSMOS optical detections to these magnitude limits is expected to be $> 99.9\%$ (Hambly et al. 2001b). The single b_J and r_F band photometry has an accuracy of $\sigma \sim$0.3 mag whereas, due to specifics of the calibration procedure, $b_J - r_F$ colors are expected to have an accuracy of $\sigma \lesssim 0.12$ mag (for details, see Hambly et al. 2001b). The 2260 candidates were then proposed for follow-up with the 6dF multifibre spectrograph. 1182 were eventually allocated fibers, mainly as secondary targets during scheduling of observations for the 6dFGS (Jones et al. 2004). Our objects were distributed over an effective non-contiguous area of $\sim$1592 deg^2.

It is important to note that our initial sample of candidates (with $J - K_s > 2$) was selected from an early version of the 2MASS Point Source Working Database. Subsequent recalibration and selection of alternate observations of some of these sources for inclusion in the final 2MASS PSC resulted in some of them having colors $J - K_s < 2$. In the end, the majority of sources classified as AGN had $J - K_s \gtrsim 1.5$, with $\sim$20% satisfying $1.5 \leq J - K_s \leq 2$ according to photometry in the public-release PSC. Uncertainties in the $J - K_s$ colors were typically $\lesssim$0.16 mag (1-σ).

3 Observations and Reduction

Spectra were obtained over the course of the 6dFGS during 2001–2006 using the UK Schmidt Telescope and the 6dF spectrograph (Watson et al. 1998; Saunders et al. 2001). For details on the 6dFGS observing strategy, see Jones et al. (2004, 2009). The primary sample for the 6dFGS was drawn from the 2MASS Extended Source Catalog (XSC; Jarrett et al. 2000). Seventeen additional (secondary) extragalactic samples were merged with the primary sample (see table 3 in Jones et al. 2009). During survey design, these were given priority indices and our initial sample of 2260 candidates had a completeness in coverage of 91.7%. This gave $\sim$6 AGN candidates per 6dF on average, although not all 6dFGS fields contained our targets because of the different galactic latitude constraints.

The 6dF multifiber spectrograph was able to record up to 120 simultaneous spectra over a 5.7° field. Each fiber has a projected diameter of 6.7 arcsec on the sky. The 2MASS positions were accurate to $\leq$0.5 arcsec and therefore light losses due to fiber positioning errors were expected to be small. For the 10th–90th percentile range in redshift for the extragalactic identifications, $z \simeq 0.15$–0.45, the fiber diameter corresponds to physical

scales of $R \simeq 17.5$ to $38.7 \, \text{kpc} \; h_{70}^{-1}$. This means the 6dF spectra sampled light from entire galaxies, and not necessarily their nuclei.

Each spectrum was taken using V and R gratings, whose outputs were later spliced to cover the effective wavelength range: ~3900–7500 Å. The observed S/N was typically 3–10 pixel^{-1}, with >10 pixel^{-1} being nominal due to the brightness of our sources. Spectra with low S/N were primarily due to poor observing conditions. The spectral resolution was typically $R \sim 1000$ throughout, corresponding to emission-line full width at half maxima (FWHM) of ~4–8 Å over the observed wavelength range. This enabled us to resolve rest-frame velocities of $\gtrsim 205 \, \text{km s}^{-1}$ over the range $z \simeq 0.15$–0.45, sufficient for AGN identification and classification.

The data were reduced, spectra extracted, and wavelength calibrated using a modified version of the Two degree Field Data Reduction (2dFDR) package developed for the 2dF Galaxy Redshift Survey. Details of the reduction are described in Jones et al. (2004) and products from the final data release (DR3; 2009 April) are described in Jones et al. (2009). The flux calibration was very crude in that the same average spectral transfer function (derived once using a couple of standards) was assumed for every 6dF observation for all time. The spectra are therefore not of spectrophotometric quality. This severely limited our classification process, e.g., using emission line ratios (see Section 4). The spectra were corrected for atmospheric absorption and emission features. However in some cases, imperfect sky-subtraction has left the imprint of the brightest sky lines.

Quality flags were assigned by the semi-automated 6dFGS redshift determination pipeline (see Section 4 for details). Almost all redshifts were visually inspected by the 6dFGS team. Quality flags in the range $Q = 1$–4 were assigned in the final public catalog[2]. $Q = 4$ represents a very reliable redshift where, typically, the median spectral S/N was ~10 pixel^{-1}. $Q = 3$ was assigned to 'likely' redshift and $Q = 2$ to 'tentative' redshift with spectra warranting further examination. We visually examined all spectra with quality flags $Q \geq 2$, although the majority of usuable spectra had $Q = 4$ and a handful had $Q = 3$. Due to the faintness of the sources in general, 750 of the 1182 spectra observed were of such poor quality that no classification was possible. Classifications were therefore secured for 432 spectra.

Figure 1 shows: the number of proposed AGN candidates (using the optical/near-IR constraints defined in Section 2); the number of 6dF spectra observed; and the number with secure spectral identifications as a function of K_s magnitude. The dearth of candidates in the faintest bin, $15 < K_s < 15.5$, is due to a combination of our optical magnitude limits and the original $J - K_s > 2$ cutoff. This cutoff implies $J \gtrsim 17$ for $K_s > 15$ and hence a fraction of sources are expected to fall below the J-band flux limit and be excluded from the candidate list. This drop was also
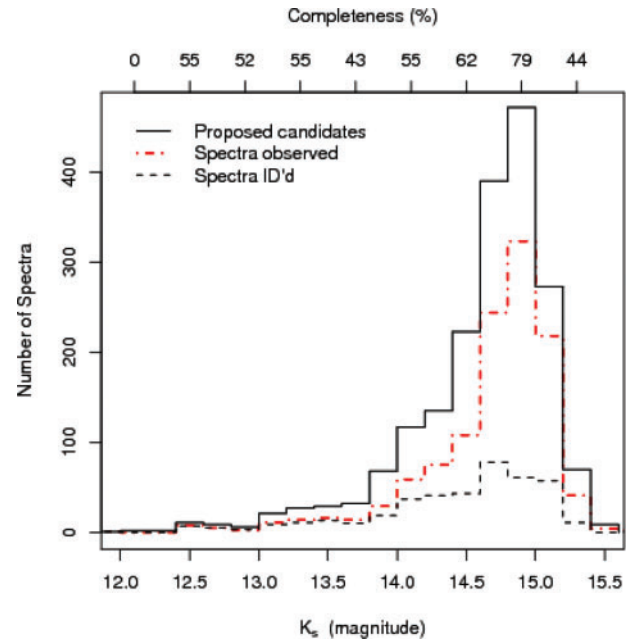

Figure 1 K_s brightness distribution of proposed AGN candidates, sources with observed spectra, and sources for which we secured a reliable spectral identification. The top horizontal axis shows the approximate completeness (= number spectra observed/number candidates) for several magnitude bins.
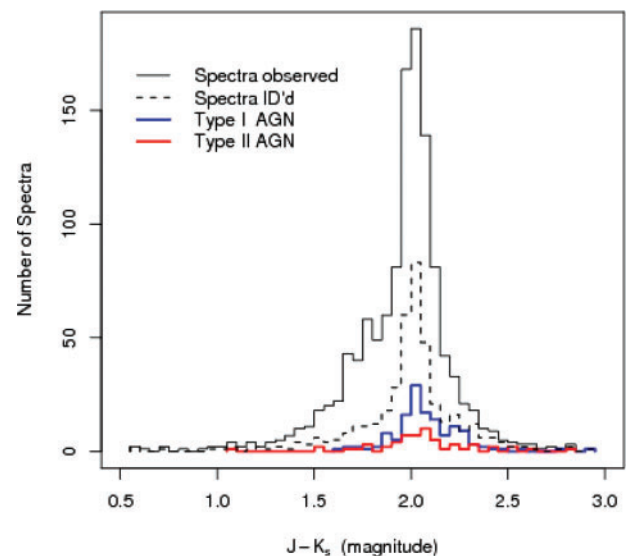

Figure 2 $J - K_s$ color distribution of sources with observed spectra, sources for which we secured a reliable spectral identification, and those identified as type I and type II AGN.

seen in the Cutri et al. (2002) sample of 704 candidates *with* follow-up optical spectroscopy. Figure 2 shows that we are not significantly biased against identifying sources with the reddest $J - K_s$ colors. In fact, the spectral identification rate as a function of $J - K_s$ is approximately uniform.

Figure 1 shows that the number of spectra observed uniformally samples the K_s distribution of candidates, i.e., the completeness is approximately uniform. However, there is relatively higher incompleteness in the number of spectra
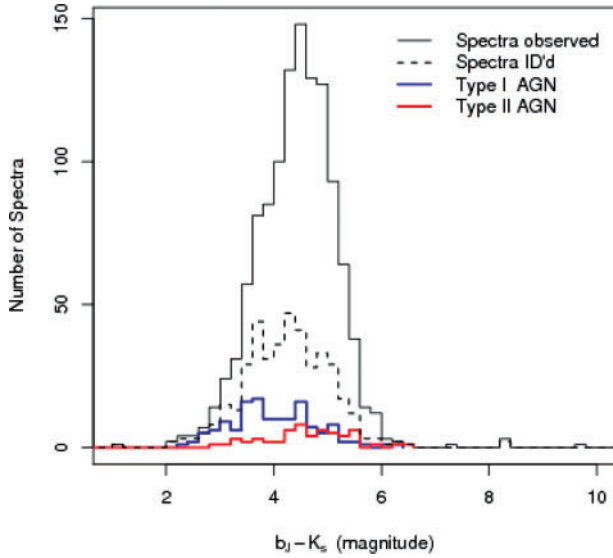
Figure 3 $b_J - K_s$ color distribution of sources with observed spectra, sources for which we secured a reliable spectral identification, and those identified as type I and type II AGN.

Table 1. Rest wavelength regions used in emission-line measurements

Line	Center[a] (Å)	Continuum integration limits (Å)	Line integration limits (Å)
[CⅢ]	1908.73	1800–1850, 1970–2010	1860–1955
MgⅡ	2798.75	2650–2700, 3000–3050	2750–2850
[OⅡ]	3728.48	3650–3700, 3770–3815	3710–3740
Hβ	4862.68	4740–4840, 4880–4940	4845–4880
[OⅢ]	5008.24	4880–4940, 5030–5100	4990–5025
Hα	6564.61	6400–6520, 6630–6700	6550–6572
[NⅡ]	6585.28	6400–6520, 6630–6700	6572–6594
[SⅡ]	6725.48[b]	6630–6700, 6745–6845	6700–6745

[a]As defined in Vanden Berk et al. (2001).
[b]Average of doublet [SⅡ] $\lambda\lambda 6718.29, 6732.67$.

identified at the faintest magnitudes, $14.5 < K_s < 15.25$. The incompleteness in this range is ∼70% with respect to the number of spectra observed. This is primarily due to the faintest sources generally having poorer quality spectra. These are expected to be near the optical magnitude limit imposed for spectroscopy, $17 \lesssim b_J \leq 18$. In fact, the introduction of an optical magnitude cut is expected to have biased the spectral sample towards bluer optical colors in general. Comparing the relative deficit in the number of faint ($K_s > 14.5$) sources to the original candidate K_s distribution (from Cutri et al. 2002) with no optical magnitude limit imposed, we estimate we have lost $\gtrsim 35\%$ of candidates due to this optical cut. A majority of these missed candidates (with $b_J > 18$) have $b_J - K_s$ colors $\simeq 4$–6. However, the *spectrally*-observed $b_J - K_s$ distribution (Figure 3) shows that we are not completely biased against identifying the reddest sources. When compared to the colors of optically selected QSOs, the 2MASS AGN have a tail extending to moderately redder colors (see Figure 10 and Section 5.2 for more details).

4 Classification

All spectra were initially classified using the semi-automated 6dFGS classification software, whose primary purpose was to determine accurate redshifts. This is a modified version of the RUNZ software used for the 2dF Galaxy Redshift Survey (Colless et al. 2001). It used 13 spectral templates to identify spectra using line-fitting and cross-correlation techniques. In general, this program produced very reliable redshifts for all galaxies, although was less reliable at separating out the various AGN classes from late- and early-type galaxies, and stars. All spectra were visually inspected to determine whether a poor-quality spectrum flagged by the 6dFGS software was worthy of further examination.

432 spectra were of sufficient quality to enable a classification of some sort, but not necessarily an unambiguous identification. All spectra were shifted to their rest frame using redshifts determined by the 6dFGS program.

4.1 Emission-Line Diagnostics

We assembled a database of emission-line diagnostics for all the good quality spectra to assist with the identifications. The diagnostics included line fluxes, equivalent widths (EWs), and dispersion velocities. These were estimated by fitting Voigt profiles and the underlying continua were approximated by linearly interpolating straight-line fits on either side of each line. Line fluxes were then determined by integrating the flux in the fitted profiles above the continuum level. Dispersion velocities were determined from the FWHM of the lines. The lines of interest and the effective wavelength regions used to define the continuum and line integration limits are shown in Table 1.

The *fitprofs* task in IRAF was used for the automated measurement of line diagnostics. This included the ability to deblend closely separated lines, e.g., Hα and [NⅡ]. An important input parameter for the *fitprofs* task is an estimate of the 1-σ uncertainty per pixel. This allows the program to compute uncertainties in each of the fitted line parameters. Since the fitting was non-linear, this was accomplished using a Monte Carlo simulation. The spectral uncertainty was computed by first selecting a relatively clean region in the rest frame common to each spectrum, i.e., devoid of strong emission and absorption lines. We selected the rest wavelength range 5050–5400 Å. We then fitted a straight line to the data in this region using a robust (outlier-resistant) regression method based on the concept of 'M-estimation' (Huber 1981). The uncertainty was then estimated using the median absolute deviation in the residuals from the fit, and is also robust against potential outliers:

$$\sigma \simeq 1.4826 \text{ median } \{|p_i - fit\{p_i\}|\}, \qquad (1)$$

where p_i is the value of the ith pixel in the 1-D spectrum and $fit\{p_i\}$ is the fitted value. This quantity is scaled
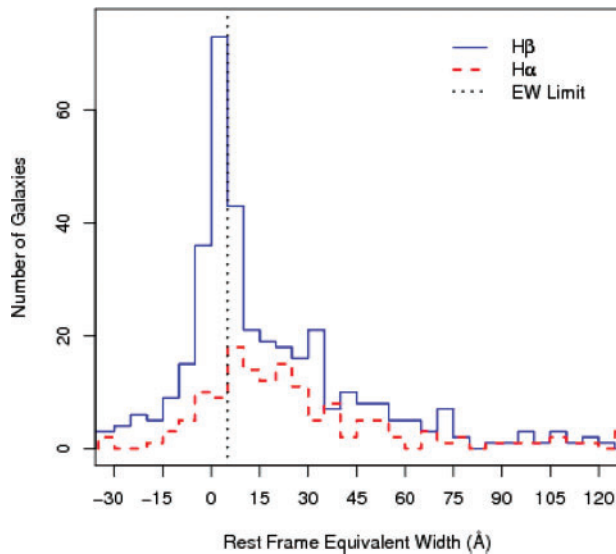
Figure 4 Distribution of rest-frame Hα and Hβ equivalent widths for all galaxies with the best quality specta. We are sensitive to all equivalent widths to the right of the vertical dotted line (>5 Å).

Figure 5 Line ratio diagram for galaxies with type I AGN classifications removed. Diamonds and filled circles are 'probable' type II AGN and star-forming galaxies, respectively, all at ≥ 0.2 dex (1-σ) from the classification boundary of Kewley et al. (2001, solid line). Crosses are composites (classified as unknown galaxies). Errors in the line ratios are typically 0.2 dex (1-σ).

such that it converges to the standard-deviation of a Gaussian in the limit of a large sample. For spectra where the range 5050–5400 Å included or fell outside the long wavelength end (λ_{red}) after shifting to the rest frame, a wavelength range of $\lambda_{red} - 250 \leq \lambda \leq \lambda_{red} - 20$ Å was used instead. In all cases, this ensured >20 pixels for the noise computation.

We estimated the smallest EW we are sensitive to by examining the dispersion in Hα and Hβ EWs of all the galaxies (and potential AGN) with the best quality spectra ($Q = 4$). Figure 4 shows these distributions. EW measurements clustered around zero are lineless galaxies where an identification would be highly unreliable, if at all possible. We found we should be sensitive to galaxies with rest-frame EW in either Hα or Hβ of $\gtrsim 5$ Å. Given our observed wavelength range, either of these lines are expected to be observed at $z \lesssim 0.5$ and therefore were used as constraints in the identification process below.

Line fluxes and EWs were also measured interactively by integrating the line fluxes directly from the 1-D spectra. These were in excellent agreement, to within measurement error, with the profile-derived fluxes from above. All lines were visually inspected and unreliable flux measurements flagged. These were primarily lines that were contaminated by a strong sky line or atmospheric absorption band. Our final emission line database retained lines with fluxes $\gtrsim 2.5\sigma$, and lines that were clearly discernable by eye in case our automated measurement of σ was overestimated. Unreliable σ estimates occured in $\simeq 7\%$ of the spectra. Note that we did not correct the emission line fluxes for any underlying absorption (e.g., from stellar photospheres) since a study using similar spectra from 2dF by Francis et al. (2004) found this effect to be negligible.

A first pass examination of the spectra together with initial classifications provided by the 6dFGS program motivated us to define six broad object classes: type I
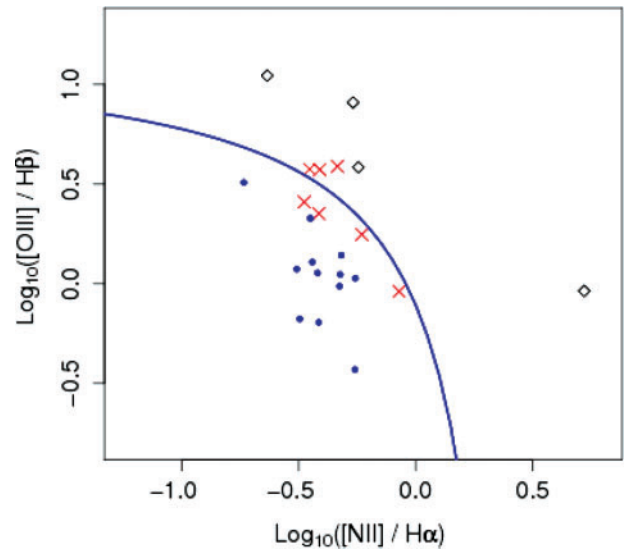
AGN; type II AGN; starburst or late-type star-forming galaxies; early-type galaxies; stars; and unknown emission line galaxies. These classes and the criteria used to identify them are as follows.

Spectra with broad Hα and/or Hβ emission lines exceeding $1000 \, \text{km s}^{-1}$ (FWHM), or with other broad permitted lines present, e.g., [CIII] or MgII for $z \gtrsim 1$ and $z \gtrsim 0.4$, respectively, were classified as type I AGN. Included in this criterion are $S/N \geq 2.5$ on the FWHM measurement and a Hα or Hβ EW > 5 Å. Spectra in which known broad lines could be discerned by eye but were relatively noisy, i.e., with flux $S/N < 2.5$ were classfied as 'probable' type I AGN.

Non-type I AGN spectra were classified using line ratios involving good measurements in either of the following line pairs: ([OIII], Hβ) or ([NII], Hα) or ([SII], Hα) or ([OIII], [OII]). We first attempted a classification using the diagnostic diagrams of Kewley et al. (2001, 2006), which are based on the classic BPT diagrams of Baldwin et al. (1981). Figures 5 and 6 show the traditional line-ratio diagrams using our good quality spectra (with pre-classified type I AGN removed) and where *all* four lines had flux $S/N \geq 2.5$. Unfortunately, all four lines in either Figure 5 or 6 were only simultaneously visible (and with good S/N) in $\simeq 8\%$ (23/296) of the good-quality non-type I spectra. Furthermore, the errors in the line ratios ($\simeq 0.2$ dex, 1-σ) were too large for the bulk of these spectra to be reliably classified. We therefore declared the few type II AGN and star-forming galaxies that could be classified using this method (at distances ≥ 1-σ from the classification boundaries) to be probable identifications.

For the remaining 273 sources with good quality data, and where only one of the above line pairs
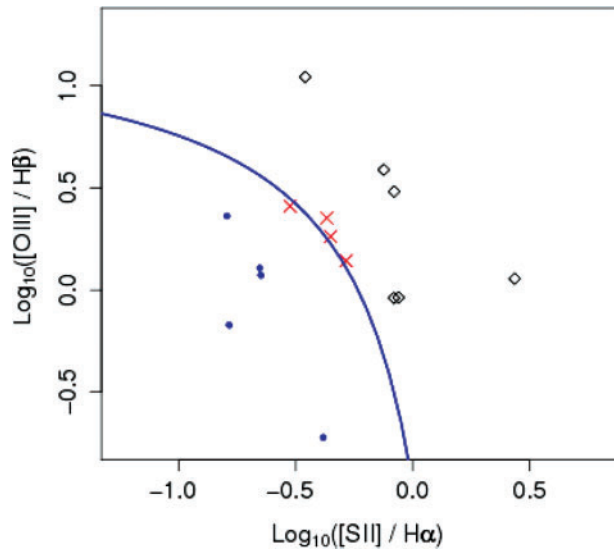
Figure 6 Line ratio diagram for galaxies with type I AGN classifications removed, but with [SII] in the abscissa. Diamonds and filled circles are 'probable' type II AGN and star-forming galaxies, respectively. The solid line is the AGN/star-formation discriminator from Kewley et al. (2001). Crosses are composites (classified as unknown galaxies). Errors in the line ratios are typically 0.2 dex (1-σ).

was available (predominately when $z \gtrsim 0.1$), a galaxy was classified as a 'probable' type II AGN if either of the following was satisfied: log([OIII]/Hβ) > 0.3 or log([NII]/Hα) > −0.2 or log([SII]/Hα) > −0.35 (e.g., Zakamska et al. 2003) or log([OIII]/[OII]) > 0 (e.g., Fraquelli & Storchi-Bergmann 2004; Kewley et al. 2006). Combined with any of these, we also required a rest-frame FWHM([OIII]) > 300 km s^{-1}, FWHM(Hα or Hβ) < 1000 km s^{-1}, and Hα or Hβ EW > 5 Å. The FWHM([OIII]) limit was included to improve the relability of type II identifications when only one line pair was available. For comparison, Zakamska et al. (2003) assumed FWHM([OIII]) > 400 km s^{-1}. We assumed 300 km s^{-1} since the distribution for FWHM([OIII]) for their entire type II sample falls off sharply at <300 km s^{-1}. In the end, this limit made little difference to the type II identification statistics.

Probable starburst/late-type starforming galaxies were classified using the negation of these single line ratios with some buffer to allow for flux errors, i.e., those with: log([OIII]/Hβ) < 0.2, or log([NII]/Hα) < −0.3, or log([SII]/Hα) < −0.4, or log([OIII]/[OII]) < −0.2.

It is important to note that the type II AGN identified using the above single line pairs could be contaminated by low-metallicity emission-line galaxies or liners, especially at low redshift. Furthermore, the non-spectrophotometric nature of our spectra could invalidate some identifications made using widely separated lines (e.g., the pair [OIII], [OII]). These classifications are therefore very tentative given the quality of our data. Hence, we declare all type II AGN identifications quoted in this paper to be probable. Follow-up with higher S/N spectral observations, preferably with better calibrated throughput as a function of wavelength, will be needed for confirmation.

Early type galaxies were identified through the characteristic 4000 Å break, a signature caused by the dearth of hot and young (usually O- and B-type) stars and strong heavy-metal absorption by stellar photospheres. Stars were isolated by first ensuring that their radial velocities were $\lesssim$150 km s^{-1}. Their spectra were then matched to templates from the ELODIE stellar library (Moultaka et al. 2004). The majority were K and M dwarf stars. All other galaxy-like spectra with Hα or Hβ EW > 5 Å but not fitting the above criteria — e.g., with single line measurements, or composites lying within 1-σ (±0.2 dex) of the type II/starburst classification boundaries in Figure 5 or 6 — were classified as 'unknown galaxies'.

4.2 Results Summary

Table 2 summarizes our source classifications. We only include our secure identifications for the type I AGN, and probable identifications (as described in Section 3) are classed as 'unknown galaxies'. Also included are statistics for type I and type II AGN from the Cutri et al. (2002) northern 2MASS AGN survey and Francis et al. (2004) southern 2MASS AGN survey. The latter is broken into two color cuts. The Cutri et al. (2002) study has at least twice the detection rate for type I AGN. This could be due to deeper spectroscopic follow-up of fainter single targets in their study. It is possible that a significant fraction of our fainter targets at K_s > 14.5 (e.g., Figure 1) could not be secured are type I AGN through spectral identification. It is also interesting to note in Table 2 that there is a tendency for the type I AGN identification rate to increase with $J − K_s$ color.

Figure 7 shows a sampling of spectra for the new type I AGN, primarily those with the highest redshifts. Two of the sources are at $z > 1$: 2MASS J21571362-4201497 with $z = 1.321$ and 2MASS J10012986-0338334 with $z = 1.389$. The latter has been classified as a probable type I AGN due to a low spectral S/N, although given its relatively high redshift, it is most likely a QSO.

Table 3 lists the secure (T1) and probable (PT1) type I AGN identifications. There are 116 classified as T1 and 20 as PT1. Previous or alternative names as listed in the NASA Extragalactic Database (NED) are given. Of the 136 type I AGN, 8 (∼6%) were previously classified as either 'AGN', 'QSO' or 'AGN/QSO?' in NED. Four of these are in the SDSS QSO sample. This implies a majority are new, previously undiscovered AGN. Interestingly, ten of our type I AGN were previously detected in X-ray by the ROSAT All-Sky Survey (RASS). Table 4 lists the type II AGN, all of which are classified as probable using the methods described in Section 3. None of the type II AGN were previously classified as AGN-like, and only one was detected in X-ray by the RASS. Of the previous classifications available in NED, a majority of our type I and II AGN are listed as galaxy-like and extended in the optical (SuperCOSMOS digitized plates) or near-IR (2MASS Atlas Images). At least 30% are also in the 2MASS Extended Source Catalog (XSC; Jarrett et al. 2000). This is expected given the depth of our sample.

Table 2. Source classifications and comparisons to previous studies

	This study $(J - K_s \gtrsim 1.7)$	Cutri et al. (2002) $(J - K_s > 2.0)$	Francis et al. (2004) $(J - K_s > 1.2)$	Francis et al. (2004) $(J - K_s > 1.8)$
Number classified	432	664	1304	66
Stars (%)	23 (5.3)[a]	66 (9.9)	330 (25.3)	6 (9.1)
Unknown galaxies (%)	193 (44.7)	…	…	…
Early-type galaxies (%)	17 (3.9)	…	…	…
SB/late-type galaxies (%)	26[c] (6.0)	…	106 (8.1)	…
Type I AGN (%)	116[b] (26.8)	385 (57.9)	14 (1.1)	4 (6.0)
Type II AGN (%)	57[c] (13.2)	100 (15.0)	23 (1.8)	0 (0.0)

[a]Values in parenthesis are percentages of the 'number classified' (first row).
[b]The 20 probable identifications are excluded here and classified as 'unknown galaxies'.
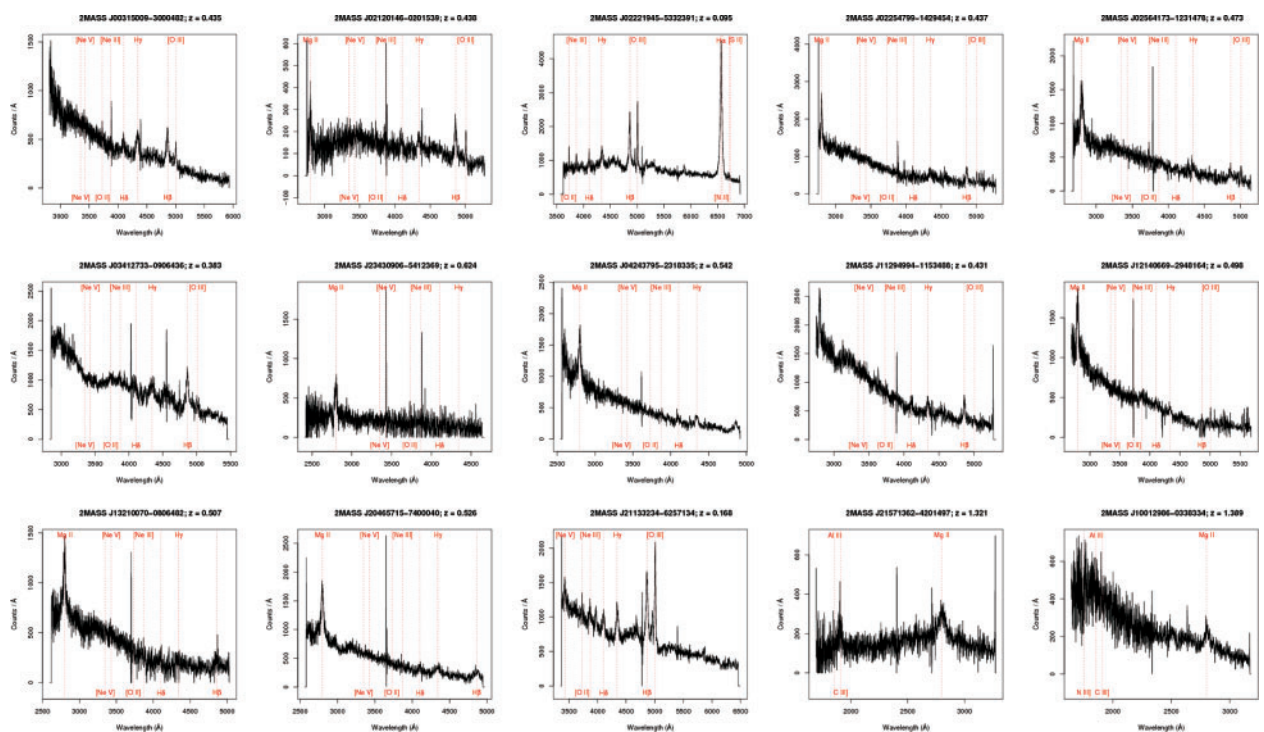[c]We declare all these to be probable identifications.

Figure 7 Rest-frame spectra of some new type I AGN overlayed with emission lines typically found in QSO spectra. The spectra for all objects listed in Tables 3 and 4 can be viewed by querying the 6dF public database: http://www.aao.gov.au/6dFGS/.

5 Discussion

This section reviews the properties of our 2MASS AGN and compares them to those of AGN/QSOs discovered in optical surveys. We explore their redshift, luminosity, photometric and line EW distributions. Our primary benchmark and comparison sample of optically-selected AGN/QSOs is the SDSS Quasar Catalog Data Release 5 (DR5; Schneider et al. 2007). This catalog contains 2MASS matches to 9824 AGN, all within 2 arcsec.

5.1 Redshift and Luminosity Distributions

Our 2MASS AGN span the range $0.01 \lesssim z \lesssim 1.38$ as shown in Figure 8a. The median z is $\simeq 0.27$ and $\simeq 0.21$ for type I and type II AGN, respectively. A majority of our

AGN are at low redshifts, with only two at $z > 0.7$. There are six securely identified AGN (four type I, two type II) at $z < 0.05$. This is 24% (6/25) of all secure *galaxy*-like spectral identifications (including unknown types) in this redshift range. This is a lower limit since some objects classified as 'unknown' could be type II AGN. Even removing our 'probable' type II AGN, the AGN fraction is still relatively high. For comparison, Hao & Strauss (2004) find $\sim$4% of $\simeq$15 200 SDSS-detected galaxies at $z < 0.05$ harbor AGN (mostly Seyferts). An earlier study by Huchra & Burg (1992) found AGN (including LINERs) in $\simeq$3.4% of a sample of 2399 nearby blue-selected galaxies. These studies are not a fair comparison since the galaxies were optically selected. It would be of interest to determine the fraction of SDSS galaxies with active nuclei for a color cut of $J - K_s > 2$.

Table 3. Type I AGN

Name	R.A.[a]	Dec.[a]	b_J	r_F	K	$J - K_s$	Redshift	ID[b]	Other name
2MASS J00004025-0541009	00 00 40.26	−05 41 00.9	17.84	16.750	13.315	2.212	0.094	T1	2MASX J00004028-0541012
2MASS J00020731-4722504	00 02 07.32	−47 22 50.5	18.52	18.190	14.909	1.999	0.389	T1	IRAS F00063-6249
2MASS J00085227-6233137	00 08 52.30	−62 33 15.3	17.27	16.530	11.825	2.252	0.184	T1	
2MASS J00114353-5033299	00 11 43.54	−50 33 30.0	18.09	16.800	13.125	2.111	0.140	T1	2MASX J00114350-5033302
2MASS J00163310-0542315	00 16 33.10	−05 42 31.4	17.61	17.070	13.299	2.113	0.237	T1	1RXS J001633.2-054227
2MASS J00202646-0254583	00 20 26.46	−02 54 58.2	17.97	17.680	14.951	1.889	0.363	T1	
2MASS J00265121-0159238	00 26 51.16	−01 59 23.7	19.36	17.720	15.020	2.026	0.319	T1	
2MASS J00315009-3000482	00 31 50.08	−30 00 48.3	17.46	17.190	14.094	2.082	0.435	T1	
2MASS J00345758-3221311	00 34 57.58	−32 21 31.2	18.77	17.590	14.303	1.997	0.186	T1	2dFGRS S440Z049
2MASS J00470010-1747025	00 47 00.05	−17 47 02.0	18.84	17.080	12.500	2.752	0.147	T1	IRAS 00444-1803
2MASS J00573811-1406173	00 57 38.12	−14 06 17.3	18.56	17.780	14.458	2.219	0.207	T1	
2MASS J00575201-3329048	00 57 52.03	−33 29 04.6	18.53	17.550	14.691	2.162	0.270	T1	1RXS J005932.7-154032
2MASS J00593208-1540302	00 59 32.11	−15 40 29.7	18.33	16.800	14.778	1.620	0.254	T1	
2MASS J01144251-5136137	01 14 42.46	−51 36 13.8	18.71	17.970	14.806	1.746	0.205	T1	
2MASS J01274593-4453170	01 27 45.95	−44 53 17.0	17.83	17.320	14.683	1.868	0.385	T1	
2MASS J01283395-2358359	01 28 33.96	−23 58 35.8	18.58	17.910	14.428	2.433	0.462	PT1	
2MASS J01290719-2356300	01 29 07.24	−23 56 30.2	19.48	17.770	15.053	1.793	0.020	T1	APMUKS B012644.60-241200.3
2MASS J01340171-5618454	01 34 01.70	−56 18 45.5	17.46	17.190	13.762	2.050	0.328	PT1	SUMSS J013401-561844
2MASS J01354636-3539148	01 35 46.35	−35 39 15.3	18.03	17.050	13.396	2.000	0.137	T1	2MASX J01354638-3539151
2MASS J01380953-0109201	01 38 09.54	−01 09 20.1	16.68	16.360	13.141	2.271	0.273	T1	SDSS J013809.53-010920.2
2MASS J01432356-0124523	01 43 23.57	−01 24 52.4	18.04	17.250	13.858	2.036	0.368	T1	
2MASS J01553002-0857040	01 55 30.03	−08 57 04.0	17.95	16.910	12.690	2.072	0.164	T1	SDSS J015530.02-085704.0
2MASS J01593068-1128584	01 59 30.69	−11 28 58.5	18.15	17.270	13.676	2.062	0.161	T1	
2MASS J01593518-2010583	01 59 35.20	−20 10 58.4	19.15	17.670	14.078	2.267	0.317	PT1	APMUKS B015713.48-202531.4
2MASS J02112824-0640013	02 11 28.22	−06 40 00.8	18.42	18.000	14.816	2.045	0.426	PT1	
2MASS J02120146-0201539	02 12 01.47	−02 01 53.8	19.20	17.720	14.182	2.163	0.438	PT1	
2MASS J02144017-6839338	02 14 40.21	−68 39 33.8	18.96	17.870	14.412	1.916	0.305	PT1	
2MASS J02155303-4709570	02 15 53.04	−47 09 57.1	17.64	16.690	12.602	2.085	0.140	T1	2MASX J02155306-4709573
2MASS J02181461-1012491	02 18 14.61	−10 12 49.1	17.86	18.170	15.054	2.036	0.568	PT1	
2MASS J02221945-5332391	02 22 19.44	−53 32 39.1	16.61	15.540	12.626	2.035	0.095	T1	
2MASS J02252283-2441528	02 25 22.84	−24 41 52.8	17.81	17.390	14.435	2.109	0.009	T1	
2MASS J02254799-1429454	02 25 48.01	−14 29 45.4	18.63	17.930	15.026	2.068	0.437	T1	
2MASS J02255003-0601450	02 25 50.04	−06 01 45.1	17.13	16.380	13.574	2.156	0.319	T1	
2MASS J02270655-3220448	02 27 06.52	−32 20 44.7	18.42	17.530	14.119	1.985	0.249	T1	2dFGRS S463Z081
2MASS J02293513-0552094	02 29 35.14	−05 52 09.4	17.47	16.940	13.928	2.280	0.293	T1	
2MASS J02313792-2308312	02 31 37.93	−23 08 31.2	15.68	15.410	12.941	2.008	0.249	T1	
2MASS J02331354-1506540	02 33 13.55	−15 06 54.1	18.69	18.060	15.059	2.035	0.337	PT1	
2MASS J02365236-5554463	02 36 52.33	−55 54 46.3	17.42	17.620	14.342	1.960	0.312	T1	
2MASS J02391868-0115211	02 39 18.69	−01 15 21.1	18.52	18.150	14.919	1.975	0.374	T1	SDSS J023918.70-011521.0
2MASS J02452486-1623432	02 45 24.86	−16 23 43.3	18.81	17.660	14.252	2.034	0.286	T1	APMUKS B024304.02-163618.0
2MASS J02460800-1132367	02 46 08.01	−11 32 36.6	16.39	16.340	13.234	2.470	0.270	T1	IRAS F02437-1145
2MASS J02535862-4558236	02 53 58.63	−45 58 23.9	18.87	17.970	14.189	2.837	0.460	PT1	
2MASS J02564173-1231478	02 56 41.72	−12 31 48.4	17.27	17.110	14.926	2.034	0.473	T1	
2MASS J02574845-0918443	02 57 48.45	−09 18 44.6	18.07	17.020	13.319	2.140	0.145	T1	2MASX J02574849-0918440
2MASS J02593835-1513092	02 59 38.35	−15 13 09.2	17.16	16.760	13.906	2.122	0.354	T1	NVSS J025938-151306

2MASS	RA	Dec							Other name
2MASS J03001 2933-1632400	03 01 29.35	−16 32 39.8	17.00	16.940	14.150	2.110	0.334	T1	
2MASS J03103479-6412052	03 10 34.80	−64 12 05.2	17.76	16.750	13.232	1.967	0.190	T1	2MASX J03103473-6412054
2MASS J03153812-0912337	03 15 38.11	−09 12 34.0	16.29	15.440	12.580	2.041	0.352	T1	
2MASS J03173580-3817251	03 17 35.81	−38 17 25.3	18.21	17.840	14.693	2.290	0.254	T1	
2MASS J03232133-2557442	03 23 21.34	−25 57 44.3	17.73	17.530	14.568	2.232	0.290	PT1	
2MASS J03261346-2018137	03 26 13.45	−20 18 13.7	18.41	17.760	14.582	2.139	0.281	T1	
2MASS J03360954-0619128	03 36 09.52	−06 19 12.9	17.99	18.420	15.181	1.662	0.438	T1	SDSS J033609.54-061913.1
2MASS J03374281-2522095	03 37 42.81	−25 22 09.5	17.41	16.910	13.660	2.270	0.273	T1	
2MASS J03412733-0906436	03 41 27.33	−09 06 43.5	16.99	16.330	13.554	1.997	0.383	T1	
2MASS J03413408-0547154	03 41 34.11	−05 47 15.4	18.37	17.170	14.595	2.007	0.137	T1	SDSS J034134.07-054715.7
2MASS J03440463-1252226	03 44 04.62	−12 52 22.6	17.93	16.700	13.001	2.230	0.093	T1	2MASX J03440465-1252222
2MASS J03561630-1237095	03 56 16.33	−12 37 09.2	17.50	17.550	14.828	1.955	0.318	T1	1RXS J035616.4-123712
2MASS J03561996-6251391	03 56 19.96	−62 51 39.1	18.16	17.270	12.617	2.948	0.108	T1	2MASX J035619 95-6251391
2MASS J04023421-3152594	04 02 34.22	−31 52 59.2	17.86	17.030	13.963	2.085	0.297	PT1	NVSS J040234-315301
2MASS J04043381-4039545	04 04 33.81	−40 39 54.6	18.65	17.860	14.525	2.006	0.623	T1	
2MASS J04170175-0309594	04 17 01.74	−03 09 59.7	18.53	17.580	14.745	2.214	0.330	T1	
2MASS J04225656-1854422	04 22 56.56	−18 54 42.3	16.89	14.410	11.605	2.209	0.064	T1	2MASX J04225654-1854424
2MASS J04243795-2318335	04 24 37.96	−23 18 33.6	18.14	17.350	14.621	2.009	0.542	T1	
2MASS J04324870-0921117	04 32 48.70	−09 21 11.6	18.58	17.690	14.000	2.133	0.216	T1	
2MASS J04332250-1422287	04 33 22.51	−14 22 28.6	17.42	16.800	13.592	2.276	0.347	T1	1WGA J0433.3-1422
2MASS J04352649-1643460	04 35 26.50	−16 43 46.0	17.30	16.310	13.828	2.031	0.098	T1	
2MASS J04360031-0405540	04 36 00.32	−04 05 54.0	18.15	17.830	14.492	2.235	0.091	T1	
2MASS J04364839-1123559	04 36 48.40	−11 23 55.9	17.38	16.770	13.720	2.129	0.207	T1	NVSS J043647-112347
2MASS J04411070-0639383	04 41 10.71	−06 39 38.3	18.73	17.430	14.706	2.241	0.312	T1	
2MASS J04433082-3508499	04 43 30.78	−35 08 49.9	18.24	17.970	14.553	2.049	0.457	T1	
2MASS J04481925-2158473	04 48 19.25	−21 58 47.1	18.57	17.400	13.408	2.209	0.111	T1	2MASX J04481922-2158468
2MASS J05022413-3546422	05 02 24.15	−35 46 42.3	18.34	17.950	14.417	1.993	0.155	T1	
2MASS J05043443-1521193	05 04 34.42	−15 21 19.3	17.21	16.760	13.768	2.200	0.390	T1	
2MASS J05063975-3416422	05 06 39.77	−34 16 42.2	18.96	17.480	14.211	1.990	0.173	T1	APMUKS B050450.33-342037.7
2MASS J05222203-4524370	05 22 21.99	−45 24 36.8	17.73	17.390	13.296	2.112	0.172	T1	1WGA J0522.3-4524
2MASS J05372445-3817586	05 37 24.48	−38 17 58.7	18.02	17.300	14.517	2.023	0.332	T1	
2MASS J10012986-0338334	10 01 29.88	−03 38 33.5	17.75	17.090	14.280	2.038	1.389	PT1	
2MASS J10264404-0425408	10 26 44.05	−04 25 40.6	16.99	16.930	14.539	2.007	0.254	T1	
2MASS J10443748-0705162	10 44 37.49	−07 05 15.9	17.25	17.340	14.163	2.085	0.301	PT1	
2MASS J11291836-2855531	11 29 18.36	−28 55 53.1	18.87	18.050	14.604	2.066	0.192	T1	
2MASS J11294994-1153488	11 29 49.93	−11 53 49.4	17.95	17.720	15.068	1.721	0.431	T1	
2MASS J12101994-1157105	12 10 19.91	−11 57 10.4	16.80	16.950	13.544	2.111	0.206	T1	LCRS B120745.5-114029
2MASS J12140669-2948164	12 14 06.69	−29 48 16.4	17.66	17.430	14.658	2.053	0.498	T1	
2MASS J12154011-2350122	12 15 40.14	−23 50 12.2	18.89	17.420	14.015	2.001	0.232	T1	2MASX J12154013-2350126
2MASS J12524011-3036579	12 52 40.12	−30 36 58.0	18.75	18.350	15.278	1.962	0.430	PT1	
2MASS J12590021-3152245	12 59 00.21	−31 52 24.5	18.66	18.080	14.090	2.327	0.292	T1	
2MASS J13210070-0806482	13 21 00.72	−08 06 47.9	17.88	17.560	14.786	2.074	0.507	T1	
2MASS J13240925-1525097	13 24 09.26	−15 25 09.4	17.69	17.320	14.754	1.917	0.531	PT1	
2MASS J13265209-1506385	13 26 52.11	−15 06 38.8	19.94	17.880	13.872	2.144	0.323	T1	
2MASS J13450643-2705409	13 45 06.44	−27 05 41.0	18.22	17.640	14.783	1.950	0.276	T1	
2MASS J13500251-2619308	13 50 02.52	−26 19 30.8	18.46	17.010	14.133	2.006	0.208	T1	2MASX J13500249-2619306
2MASS J14403905-1927129	14 40 39.05	−19 27 13.0	18.21	17.400	14.264	2.251	0.295	T1	

(Continued)

Table 3. (Continued)

Name	R.A.[a]	Dec.[a]	b_J	r_F	K	$J - K_s$	Redshift	ID[b]	Other name
2MASS J15400255-1451363	15 40 02.54	-14 51 36.3	19.03	17.670	14.783	1.868	0.193	T1	
2MASS J15470139-0632099	15 47 01.41	-06 32 09.9	18.34	17.420	14.127	2.048	0.252	T1	
2MASS J15475594-0610480	15 47 55.95	-06 10 48.3	18.29	17.460	14.539	1.877	0.129	T1	
2MASS J20202833-3014140	20 20 28.33	-30 14 14.2	19.63	17.930	13.939	2.204	0.196	T1	
2MASS J20223079-3236086	20 22 30.79	-32 36 08.6	17.45	16.950	13.069	2.030	0.142	T1	
2MASS J20331662-2253169	20 33 16.62	-22 53 17.0	18.59	17.330	13.467	2.109	0.131	T1	PKS 2030-23
2MASS J20344129-5126573	20 34 41.28	-51 26 57.3	17.81	16.400	12.772	2.024	0.128	T1	2MASX J20344130-5126572
2MASS J20345400-3131563	20 34 53.99	-31 31 56.4	18.35	17.310	14.332	1.842	0.202	T1	
2MASS J20400728-5237227	20 40 07.30	-52 37 22.6	17.00	15.980	12.532	2.325	0.128	T1	2MASX J20400731-5237224
2MASS J20465715-7400040	20 46 57.15	-74 00 04.1	17.46	17.680	14.345	2.189	0.526	T1	PKS 2041-741
2MASS J20585386-2409418	20 58 53.86	-24 09 41.8	19.10	17.700	14.212	2.038	0.294	PT1	
2MASS J21071766-5503097	21 07 17.66	-55 03 10.1	18.60	18.010	14.117	2.374	0.461	PT1	SUMSS J210717-550308
2MASS J21132600-6316184	21 13 26.04	-63 16 18.4	18.49	17.780	14.172	2.075	0.255	T1	
2MASS J21133234-6257134	21 13 32.35	-62 57 13.5	17.67	17.010	13.545	2.066	0.168	T1	
2MASS J21260042-2558396	21 26 00.42	-25 58 39.6	18.73	17.900	14.894	1.873	0.343	T1	
2MASS J21333132-6120301	21 33 31.31	-61 20 30.2	18.32	17.590	13.840	2.062	0.116	T1	
2MASS J21570360-7322204	21 57 03.61	-73 22 20.5	17.82	16.640	13.033	1.967	0.096	T1	2MASX J21570361-7322205
2MASS J21571362-4201497	21 57 13.61	-42 01 49.2	18.64	17.910	14.562	1.888	1.321	T1	LCRS B215408.7-421607
2MASS J21572015-4036138	21 57 20.17	-40 36 13.8	17.77	17.820	14.058	2.359	0.301	T1	
2MASS J21572316-3123064	21 57 23.17	-31 23 06.5	16.50	15.640	12.469	2.151	0.085	T1	1RXS J215723.3-31230
2MASS J22161121-3947337	22 16 11.23	-39 47 33.7	18.35	16.500	13.920	2.004	0.246	T1	
2MASS J22165321-4451568	22 16 53.21	-44 51 57.0	15.83	15.340	12.421	2.067	0.135	T1	LCRS B221349.8-450657
2MASS J22170559-3619460	22 17 05.60	-36 19 46.1	17.58	17.120	13.687	2.040	0.151	T1	
2MASS J22180018-3957228	22 18 00.19	-39 57 22.7	17.83	16.640	13.177	2.072	0.244	T1	
2MASS J22212645-4757598	22 21 26.46	-47 57 59.6	17.97	17.970	14.520	1.969	0.198	T1	
2MASS J22250207-1841401	22 25 02.09	-18 41 40.0	17.50	17.540	14.573	2.080	0.302	T1	
2MASS J22253449-1939566	22 25 34.50	-19 39 56.6	19.38	17.910	14.805	2.253	0.364	PT1	
2MASS J22385748-0539206	22 38 57.49	-05 39 20.6	18.62	16.750	13.425	2.130	0.174	T1	1WGA J2238.9-0539
2MASS J22423001-2745299	22 42 30.02	-27 45 29.6	19.58	17.740	14.773	1.695	0.199	T1	
2MASS J22431660-2020570	22 43 16.59	-20 20 57.1	18.19	17.990	14.849	2.202	0.276	T1	
2MASS J22433493-3928397	22 43 34.94	-39 28 39.6	19.10	17.630	14.025	2.042	0.217	T1	APMUKS B224042.73-394424.8
2MASS J22553836-0245335	22 55 38.34	-02 45 33.1	18.48	17.730	14.764	1.812	0.273	T1	1WGA J2255.6-0245
2MASS J22573178-0651513	22 57 31.79	-06 51 51.2	17.42	17.370	14.731	1.926	0.317	T1	
2MASS J23054834-0314121	23 05 48.29	-03 14 11.7	18.59	17.810	14.175	2.600	0.318	T1	
2MASS J23062901-4951453	23 06 29.01	-49 51 45.3	18.12	17.670	14.417	1.962	0.118	T1	
2MASS J23180937-1125452	23 18 09.36	-11 25 45.5	17.49	17.230	14.745	1.866	0.042	T1	
2MASS J23253138-3010560	23 25 31.39	-30 10 56.1	19.29	15.010	10.999	2.447	0.417	PT1	
2MASS J23305477-0956480	23 30 54.78	-09 56 48.1	18.35	17.630	14.190	1.997	0.250	T1	2MASX J23305473-0956479
2MASS J23342108-1421319	23 34 21.12	-14 21 31.3	16.67	17.020	13.971	1.861	0.243	T1	1RXS J233421.6-142128
2MASS J23352324-3945052	23 35 23.26	-39 45 05.2	18.40	17.770	14.884	1.960	0.019	T1	
2MASS J23430906-5412369	23 43 09.09	-54 12 36.8	17.81	18.230	14.609	2.189	0.624	PT1	SUMSS J234308-541238
2MASS J23441698-3322367	23 44 16.95	-33 22 36.4	18.97	18.120	14.693	2.312	0.233	T1	
2MASS J23524661-2116467	23 52 46.60	-21 16 46.9	17.30	17.120	14.751	1.937	0.280	T1	1RXS J235247.1-211644
2MASS J23582823-2259320	23 58 28.22	-22 59 31.9	18.09	16.230	13.415	2.006	0.114	PT1	2MASX J23582823-2259322

[a]In J2000.0, units are h, min, s for R.A., and deg, arcmin, arcsec for Dec.
[b]T1 = securely identified type I AGN; PT1 = probable identification.

Table 4. Type II AGN

Name	R.A.[b]	Dec.[b]	b_J	r_F	K	$J - K_s$	Redshift	Other name
2MASS J000041584-4938500	00 04 15.83	−49 38 50.2	18.75	17.420	14.399	1.776	0.199	2MASX J00041588-4938507
2MASS J001112456-0808506	00 11 24.57	−08 08 50.6	19.92	17.560	14.775	2.069	0.136	APMUKS B000851.08-08252
2MASS J001153042-0750548	00 15 30.43	−07 50 54.7	19.27	17.780	14.217	2.080	0.178	2MASX J00153041-0750549
2MASS J002137437-3726445	00 21 37.41	−37 26 44.8	18.75	17.450	14.304	2.254	0.197	
2MASS J002405501-1540006	00 24 05.51	−15 40 00.4	19.07	17.680	13.926	2.099	0.241	NVSS J002405-154004
2MASS J010232001-2151264	01 02 31.99	−21 51 26.6	12.24	14.830	14.890	1.065	0.040	2MASX J01023199-2151267
2MASS J012204245-5355324	01 22 04.19	−53 55 33.1	18.89	17.710	14.606	2.006	0.316	APMUKS B012002.43-541113.6
2MASS J012318242-2207033	01 23 18.25	−22 07 03.2	19.55	17.830	14.031	2.060	0.388	
2MASS J012652294-4556045	01 26 52.28	−45 56 04.5	19.77	17.810	14.903	1.508	0.294	IRAS F01247-4611
2MASS J012910454-4331345	01 29 10.46	−43 31 34.6	20.26	17.830	14.823	2.003	0.282	
2MASS J014136241-1747177	01 41 36.25	−17 47 17.6	17.83	17.260	14.477	1.795	0.311	
2MASS J021717791-2638482	02 17 17.90	−26 38 48.3	19.16	17.900	14.775	2.140	0.201	
2MASS J023333333-0635397	02 33 33.33	−06 35 39.5	19.10	17.570	14.403	2.051	0.185	
2MASS J023401157-1934369	02 34 01.59	−19 34 37.1	17.96	17.730	15.105	1.932	0.346	
2MASS J023457773-3349442	02 34 57.73	−33 49 44.4	18.37	16.580	14.802	1.756	0.117	2dFGRS S518Z006
2MASS J031436800-0557035	03 14 36.79	−05 57 03.2	18.15	17.520	14.739	2.124	0.107	APMUKS B031208.24-060810.4
2MASS J032325912-2110586	03 23 25.90	−21 10 58.7	19.41	17.970	14.648	1.989	0.352	
2MASS J033403661-1454428	03 34 03.66	−14 54 43.0	18.63	17.670	13.928	1.967	0.167	APMUKS B033144.22-150442.8
2MASS J034746932-2424458	03 47 46.90	−24 24 45.8	18.59	18.160	15.214	1.674	0.272	
2MASS J035356491-1605395	03 53 56.48	−16 05 39.9	19.90	17.390	15.057	1.964	0.066	
2MASS J040439511-0930307	04 04 39.52	−09 30 30.7	18.75	17.160	14.952	2.402	0.359	
2MASS J040823802-2152363	04 08 23.81	−21 52 36.3	19.93	17.600	13.498	2.636	0.207	
2MASS J041926420-0600032	04 19 26.42	−06 00 03.3	19.06	17.880	14.601	1.952	0.223	
2MASS J042216652-2315307	04 22 16.65	−23 15 30.9	18.96	18.100	14.758	1.914	0.156	APMUKS B042009.08-232228.6
2MASS J042425303-3604244	04 24 25.30	−36 04 24.6	18.35	17.210	13.047	2.825	0.150	IRAS F04226-3611
2MASS J044020183-0802175	04 40 20.18	−08 02 17.4	19.32	17.960	13.916	2.070	0.189	2MASX J04402018-0802174
2MASS J044738694-1245944	04 47 38.70	−41 24 59.4	19.04	17.380	13.550	2.003	0.226	2MASX J04473873-4124592
2MASS J045451293-3513006	04 54 51.28	−35 13 00.9	19.29	17.860	14.256	2.208	0.240	
2MASS J045620391-1701279	04 56 20.41	−17 01 28.0	18.54	17.500	14.188	1.941	0.188	
2MASS J045708512-2415069	04 57 08.53	−24 15 06.7	19.30	17.760	14.445	2.518	0.360	
2MASS J050032086-6032458	05 00 32.09	−60 32 45.8	19.67	17.650	14.153	2.216	0.317	

(*Continued*)

Table 4. (Continued)

Name	R.A.[b]	Dec.[b]	b_J	r_F	K	$J - K_s$	Redshift	Other name
2MASS J05015803-2604343	05 01 58.04	−26 04 34.2	17.21	16.630	14.043	2.007	0.037	2MASX J05015805-2604341
2MASS J05142233-2227103	05 14 22.32	−22 27 10.4	18.41	17.930	15.160	1.966	0.357	
2MASS J05302635-3452048	05 30 26.35	−34 52 04.9	19.28	17.350	12.922	2.307	0.298	NVSS J053026-345207
2MASS J05513207-5655295	05 51 32.04	−56 55 29.5	19.17	17.660	13.908	2.140	0.257	PKS 0550−569
2MASS J09490740-1211328	09 49 07.42	−12 11 32.8	17.81	17.250	13.624	2.323	0.093	
2MASS J10505072-1000060	10 50 50.71	−10 00 05.9	18.53	17.570	14.223	2.123	0.193	NVSS J105050-100001
2MASS J11072722-0125110	11 07 27.22	−01 25 11.0	18.63	17.520	14.135	1.894	0.169	2MASX J11072722-0125117
2MASS J11575615-0453498	11 57 56.19	−04 53 49.4	19.03	17.760	15.378	1.513	0.190	
2MASS J12294408-1009001	12 29 44.07	−10 09 00.2	19.71	17.950	14.224	2.323	0.268	NVSS J122944-100900
2MASS J13021118-1201264	13 02 11.17	−12 01 26.6	18.56	17.320	14.061	2.450	0.191	2MASX J13021117-1201265
2MASS J14144317-1556194	14 14 43.16	−15 56 19.3	19.57	17.960	14.370	1.904	0.212	
2MASS J14255845-1553274	14 25 58.46	−15 53 27.5	19.37	17.940	14.377	2.235	0.284	LCRS B144720.8-024932
2MASS J14495686-0301555	14 49 56.88	−03 01 55.6	18.68	17.580	14.481	2.085	0.246	SDSS J152504.19-011156.5
2MASS J15250421-0111569	15 25 04.23	−01 11 57.2	18.66	17.750	14.799	2.048	0.123	
2MASS J15320140-0858124	15 32 01.40	−08 58 12.4	19.25	17.970	14.694	2.077	0.157	2MASX J20473225-4841082
2MASS J20473227-4841084	20 47 32.27	−48 41 08.5	18.32	16.920	13.682	2.163	0.145	
2MASS J21011126-2143329	21 01 11.26	−21 43 33.1	18.21	17.530	13.698	2.065	0.304	APMUKS B212523.73-625150.2
2MASS J21291755-6238414	21 29 17.55	−62 38 41.4	18.94	18.090	15.003	2.037	0.232	RX J2130.2-0156
2MASS J21300805-0155571	21 30 08.05	−01 55 57.1	19.75	17.950	14.793	2.107	0.290	2MASX J2138199-1001522
2MASS J21381991-1001522	21 38 19.93	−10 01 52.2	18.72	17.530	14.174	1.958	0.206	APMUKS B214245.16-293329.4
2MASS J21454002-2919369	21 45 40.02	−29 19 36.9	19.44	17.410	14.094	2.009	0.341	
2MASS J21462665-4212558	21 46 26.65	−42 12 56.1	18.96	17.830	15.181	1.877	0.209	APMUKS B220006.09-111022.8
2MASS J22024635-1055517	22 02 46.36	−10 55 51.0	18.83	17.430	12.847	2.526	0.238	
2MASS J22060976-3558119	22 06 09.70	−35 58 12.1	20.20	17.980	14.999	1.702	0.056	
2MASS J23200024-4309095	23 20 00.23	−43 09 09.5	19.01	17.670	14.096	2.054	0.177	2MASX J23200025-4309100
2MASS J23572052-5503091	23 57 20.53	−55 03 09.3	19.23	17.720	14.809	1.989	0.300	

[a]All these are probable identifications (see Section 4.1).
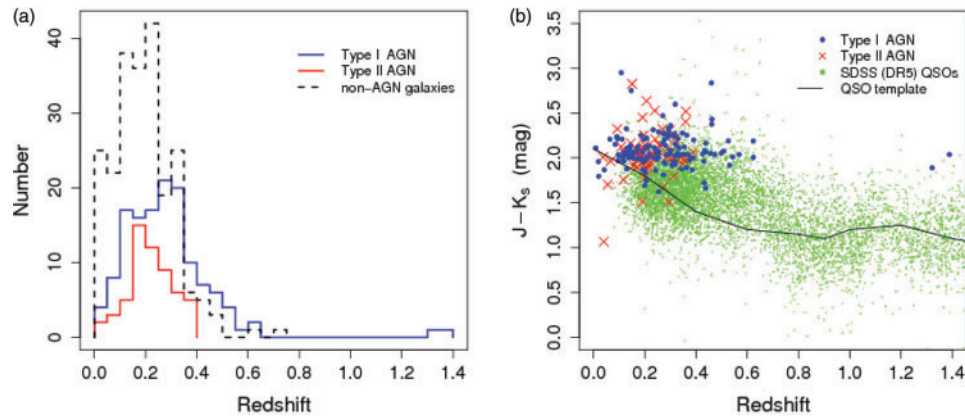[b]In J2000.0, units are h, min, s for R.A., and deg, arcmin, arcsec for Dec.

Figure 8 (a) Redshift distributions for our type I and II AGN, and inactive galaxies with good quality spectra including 'unknown' galaxies. (b) $J - K_s$ color versus redshift for our type I and II AGN, and SDSS QSOs. The line shows the prediction for radio-quiet QSOs using the template of Elvis et al. (1994). Uncertainties in $J - K_s$ are $\lesssim 0.16$ mag (1-σ).

We have a significantly higher AGN identification rate than any previous low redshift galaxy sample. This is expected to be due to our red $J - K_s$ color selection. The Francis et al. (2004) survey of 2MASS AGN had a bluer color cut, $J - K_s > 1.2$, and had a significantly lower AGN fraction (see Section 4.2 and Table 2). Evidence for (low-luminosity) AGN activity was recently found in 17% of a sample of 64 late-type spiral galaxies by Desroches & Ho (2009) using X-ray data from Chandra. Wilkes et al. (2002) and Kuraszkiewicz et al. (2009) also showed that the 2MASS red AGN are generally weak X-ray emitters, with the reddest $J - K_s$ sources being the weakest. AGN with low luminosities are therefore more common than previously thought.

Another consideration is that the 6dF fiber diameter corresponds to sampling physical scales of $R > 12.3$ kpc h_{70}^{-1} at $z \geq 0.1$. This means the 6dF spectra are sampling light from entire galaxies, even at the lowest redshifts. Furthermore, we are only sensitive to AGN with Hα or Hβ EW > 5 Å. Ho et al. (1997) showed that we are likely to miss many AGN at this EW limit within our large aperture. From spectral observations of the nuclear regions ($\lesssim 200$ pc) of a large sample of blue-selected nearby galaxies, they found that almost 50% contain active nuclei. Even though galaxy light can significantly dilute the contribution from an AGN, we find that a near-IR selected sample with a red color cut can reduce the fraction of objects whose SEDs are dominated by host galaxy light, contrary to the claim of Ho et al. (1997).

Our redshift distribution is consistent with that from Cutri et al. (2002) who used a similar $J - K_s$ color cut. They detected two QSOs with $z > 2.3$, consistent with an enhancement of the K_s band flux from Hα emission moving into that band. Figure 8b shows $J - K_s$ versus redshift for our AGN and SDSS QSOs. This shows that our red near-IR color criterion is biased towards AGN selection in low-redshifts because of the k-correction effect of the AGN/QSO SED. Most AGN show a sharp rise in flux in the rest frame between 1 and 2 μm, possibly from hot

dust emission (e.g., Sanders et al. 1989), and this is red-shifted out of the K_s band at $z \gtrsim 0.5$. The $J - K_s$ colors of SDSS QSOs and the prediction for radio-quiet QSOs from the template of Elvis et al. (1994) confirm this trend. Barkhouse & Hall (2001) showed that 2MASS has the sensitivity to detect QSOs with $J - K_s > 1.5$ out to $z \simeq 4$, maybe higher (see their figure 5), although they are very rare.

Figure 9 compares the K_s flux and luminosity between active and inactive galaxies as a function of redshift. We assumed a power-law SED $f_\nu \propto \nu^{-\alpha}$ for the k-correction. The slope α was derived from the $J - K_s$ color of each source. No foreground redenning correction was applied since the extinction is typically $A_K < 0.05$ mag for galactic latitudes $|b| > 30°$ (Schlegel et al. 1998).

Figure 9b shows that the near-infrared luminosities of some of our active galaxies are comparable to those of securely identified inactive galaxies. These are a mixture of early-type and late-type starburst galaxies, and their near-IR emission is dominated by the less-luminous host galaxy. Our AGN have a tail extending to higher luminosities (by $\simeq 2$ mag) than the inactive galaxies. This trend has been found by many authors at other wavelengths (e.g., Huchra & Burg 1992; Hao & Strauss 2004). Also, host galaxy emission could be non-negligible in the type II AGN, suggesting they would be slightly less-luminous than the type I AGN. This luminosity dependence is consistent with the observation that the fraction of type I AGN in our sample increases with redshift relative to inactive galaxies and there is a dearth of type II AGN at $z > 0.4$. For comparison, the bulk of the type I AGN extend to $z \simeq 0.6$.

The K_s luminosities of our 2MASS AGN generally overlap with those of SDSS QSOs in the same redshift range, but the bulk at $z > 0.2$ are more luminous on average than the locus formed by the SDSS QSOs (Figure 9b). Our AGN therefore have luminosities closer to QSOs than Seyferts, although we caution that the SDSS QSOs and 2MASS AGN were selected using entirely different techniques. Figure 9a shows that our AGN have a K_s flux limit
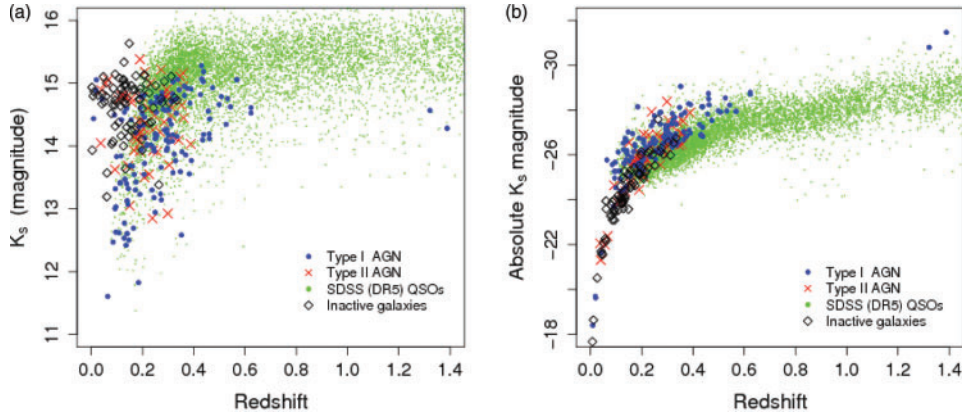
Figure 9 Apparent K_s magnitude (a) and absolute K_s magnitude (b) as a function of redshift for 2MASS AGN, SDSS QSOs, and *securely* identified inactive galaxies in our sample where 'unknown' classifications were omitted.
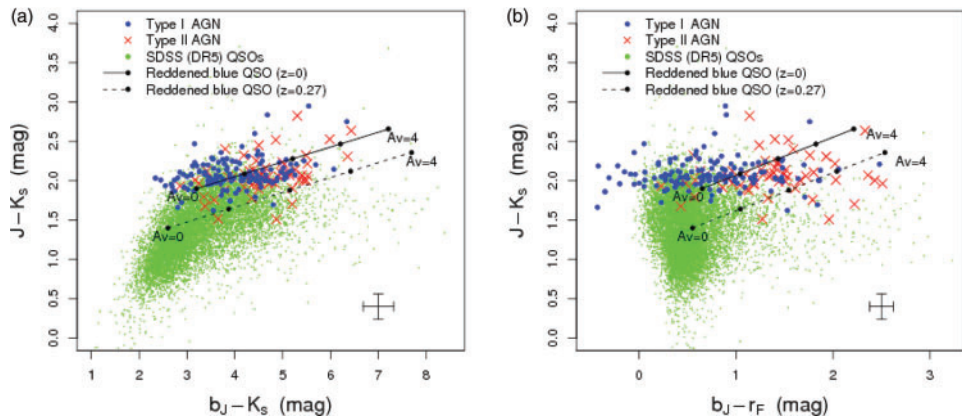

Figure 10 Color-color plots involving b_J, r_F, J, K_s for 2MASS red AGN and SDSS QSOs. The lines with filled dots indicate changes in colors due to pure dust reddening of a fiducial blue QSO assuming a $1/\lambda$ extinction law at $z = 0$ (solid lines), and at the median redshift of our type I AGN, $z = 0.27$ (dashed lines). These predictions assume the intrinsic (unreddened) colors of a QSO from the median composite of Elvis et al. (1994). The vertical/horizontal lines denote (maximum) 1-σ uncertainties along each axis: $\simeq 0.32$, 0.12, and 0.16 mag for $b_J - K_s$, $b_J - r_F$, and $J - K_s$, respectively.

($K_s = 15.5$) brighter by $\gtrsim 0.5$ mag than the bulk of SDSS QSOs at similar redshifts. A large fraction of the SDSS QSOs at $z \gtrsim 0.2$ are detected to fainter K_s magnitudes. The lower number of 2MASS AGN at $K_s > 15$ is due to the higher incompleteness in spectral identifications at the faintest magnitudes. We are therefore sensitive to the most near-IR luminous objects of the optically selected QSO population.

The ratio of type I to type II AGN in our sample is $\simeq 2{:}1$. This ratio cannot be compared to studies at other wavelengths due to the high level of incompleteness in our sample brought about by, e.g., the relatively bright optical cut imposed by spectroscopy (see Section 3). However, compared to previous 2MASS AGN studies that performed follow-up spectroscopy to similar optical limits, there is tentative evidence that the type I to type II ratio depends on $J - K_s$ color, in the sense that a redder color cut has a higher proportion of type I AGN. For example, Francis et al. (2004) find ratios of 14:23 and 4:0 for $J - K_s > 1.2$ and > 1.8, respectively, and Cutri et al. (2002) found $\simeq 4{:}1$ for $J - K_s > 2$ (Table 2). We find $\simeq 2{:}1$

for an effective $J - K_s \gtrsim 1.7$. All these studies follow the same qualitative trend and cannot be explained by redshift or luminosity dependent biases. This is consistent with the notion that most type II AGN (e.g., Seyferts 2s) have their optical-to-near-IR emission dominated by 'blue' host galaxy light, and that a red $J - K_s$ cut will select more sources where the active nuclear emission dominates, i.e., type I AGN and QSOs at moderately low redshift.

5.2 Broadband SEDs and Dust Reddening

Figure 10 compares the optical-to-near-IR colors of 2MASS red AGN to those of SDSS QSOs. The SDSS optical magnitudes were converted to equivalent UKST photographic b_J, r_F magnitudes by first converting them to Cousins B, V using the color corrections in Fukugita et al. (1995), and then to UKST magnitudes (on the Vega system) using the corrections in Blair & Gilmore (1982). Overall, the type I AGN span a range in $b_J - K_s$ and $b_J - r_F$ color similar to those of optically-selected SDSS QSOs at the same $J - K_s$ color cut. This is not surprising because our sample required a relatively bright optical

magnitude cut for reliable follow-up spectroscopy (see Section 2). We could indeed be sampling the same AGN population detected in the optical and spanning the same (low) redshift range (Figure 8b). Interestingly, the spread in $b_J - K_s$ and $b_J - r_F$ of the 2MASS red AGN are also consistent with the radio-loud quasar selected samples of Webster et al. (1995) and Francis et al. (2000), although these samples spanned a large range in redshift and very few sources were detected in all 2MASS bands.

The type II AGN have redder optical colors than the bulk spanned by type I AGN (Figure 10b) where $\Delta(b_J - r_F) \simeq 1$ mag. This is consistent with the AGN unified model where our view to the nuclear region is completely obscured and red host galaxy light will dominate the continuum flux at all wavelengths. The starlight can be instrisically red (e.g., evolved stars), reddened by dust, or both. Type I AGN have bluer optical colours, consistent with the SDSS QSOs. The optical properties of 2MASS red type I AGN are therefore not dramatically different from those in optically selected samples.

Our spectral observations are not sufficiently spectrophotometric to warrant use of emission line ratios to constrain the amount of dust reddening. However, the distribution of optical and near-IR colors does not exclude mild amounts of dust reddening. Figure 10 shows reddening vectors for dust with an optical depth $\tau_\lambda \propto 1/\lambda$ applied to the colors of a typical blue QSO in the rest frame ($z = 0$) and as observed at the median redshift of our type I AGN ($z = 0.27$). In order for a 'blue' QSO to be promoted to the region of color space occupied by the 2MASS red type I AGN, we require extinctions of $A_V < 2$ mag. Note that there is evidence that the color-color locus occupied by the SDSS QSOs may already be extended by dust reddenning with $A_V \lesssim 1.5$ mag (Richards et al. 2003). This is to be compared to QSOs discovered in earlier optical/UV surveys that used more rigid selection criteria. For example, the LBQS (Hewett et al. 1995) spans $0.6 \lesssim J - K_s \lesssim 1.4$, $2 \lesssim b_J - K_s \lesssim 4$, and $0.5 \lesssim b_J - r_F \lesssim 1.5$, considerably bluer than the SDSS QSOs. Using the LBQS as an unreddened comparison sample would make the 2MASS AGN colors more difficult to reconcile with a simple screen extinction model with $\tau_\lambda \propto 1/\lambda$. Most of the 2MASS AGN are too blue in their optical colors for dust to be wholly responsible for modifying their optical/near-IR continua relative to blue-selected QSOs.

However, there is some evidence that at least some 2MASS AGN are reddened by dust. The SEDs for a sample of ten very red 2MASS AGN with $J - K_s > 2$, $R - K_s > 5$, $b_J - K_s \gtrsim 5.5$ were modeled by Georgakakis et al. (2009). They found that all sources were consistent with moderate amounts of dust reddenning of $A_V = 1.3$–3.2 mag. They also found that the mid-IR SEDs are dominated by hot dust and that their $60/12\,\mu$m luminosity ratios are significantly higher than those of blue-selected Palomar-Green (PG) QSOs (Schmidt & Green 1983), suggesting a higher level of star-formation. Similar conclusions were reached by Kuraszkiewics et al. (2009), including evidence that in a handful of highly polarized
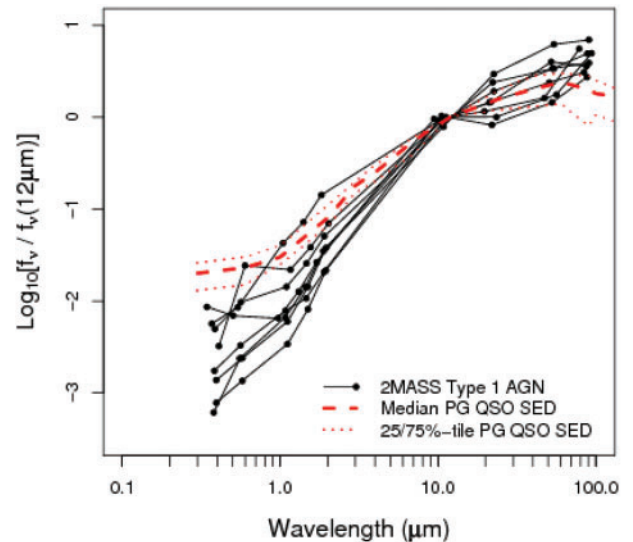

Figure 11 Rest-frame SEDs of Infrared Astronomical Satellite (IRAS) detected 2MASS type I AGN (dots connected with lines) and the median, 25th, and 75th percentiles of PG QSO SEDs from Georgakakis et al. (2009, dashed and dotted lines). These authors used survival statistics to account for upper limits in the flux measurements of PG QSOs. All SEDs are normalized to a linearly interpolated rest-frame 12 μm flux density.

objects the optical has a contribution from AGN light scattered by dust.

We repeated a similar analysis as in Georgakakis et al. (2009) to determine whether our 2MASS red AGN have a significantly higher far-IR emission on average. A search through the Spitzer and ISO archives revealed no mid-to-far IR data. However, eight type I AGN were securely detected by IRAS in all bands (12, 25, 60, and 100 μm). One of these (2MASS J04225656-1854422) was previously identified as a Seyfert 1 galaxy, another (2MASS J02460800-1132367) was also detected in the RASS as an ultra-luminous IR galaxy, and the remainder are given a 'galaxy' classification in NED. The eight IRAS all-band-detected AGN span redshifts $0.06 \leq z \leq 0.27$ and are at the red end of the $b_J - K_s$ color distribution with $b_J - K_s \gtrsim 4.5$. Photometry was extracted from the IRAS Faint Source Catalog v2.0 using the IPAC Infrared Science Archive. In fact, only 10% of our 2MASS AGN (both type I and II) were detected in at least one band by IRAS, indicating the 2MASS red AGN are not predominately associated with the ultraluminous IR QSOs found by Low et al. (1988).

Figure 11 shows the *rest-frame* optical-to-far-IR broadband SEDs (at $b_J, r_F, J, H, K_s, 12, 25, 60, 100\,\mu$m) of this subsample of 2MASS AGN. The SEDs are normalized to the rest-frame 12 μm flux density since this wavelength is expected to be a relatively unbiased indicator of AGN power (e.g., Spinoglio & Malkan 1989), i.e., independent of dust extinction and star formation rate. The rest-frame 12 μm flux density was estimated by linearly interpolating between the $12/(1 + z)$ and $25/(1 + z)$ wavelengths in the
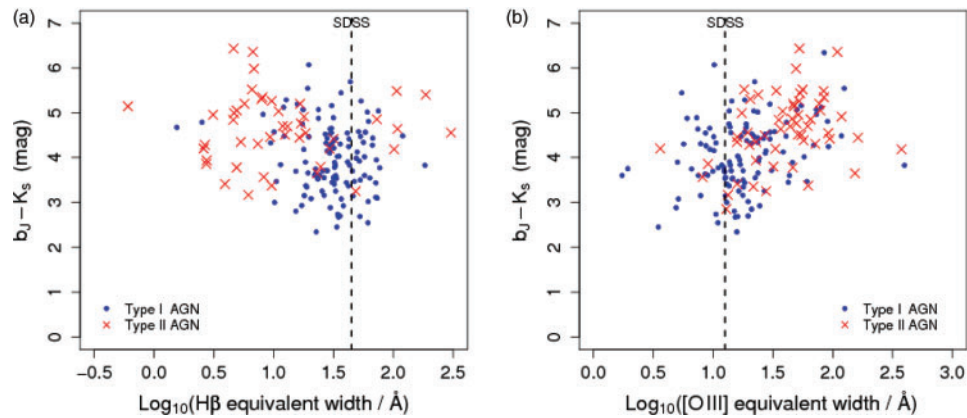
Figure 12 $b_J - K_s$ color as a function of rest-frame Hβ equivalent width (a) and rest-frame [OIII] equivalent width (b) for the 2MASS type I and II AGN. Dashed vertical lines show equivalent widths from the SDSS median composite spectrum of Vanden Berk et al. (2001). 1-σ uncertainties are $\lesssim 0.32$ mag in $b_J - K_s$ and $\lesssim 0.18$ in $\log_{10}$(EW).

rest frame. Figure 11 also shows the spread (25th–75th percentile range) observed for optically selected PG QSOs. These lines are directly from Georgakakis et al. (2009). The 2MASS red AGN all have higher normalized rest-frame far-IR emission at $\lambda \gtrsim 80\,\mu\text{m}$ than the PG QSOs (at >95% significance). Three 2MASS AGN also have higher emission at rest-frame wavelengths $50\,\mu\text{m} < \lambda < 60\,\mu\text{m}$. This indicates the far-IR emission in at least a handful of 2MASS AGN is dominated by heated dust, either due to star formation, the central AGN or both. This same dust could contribute to redenning of their optical-to-near-IR continua. It's important to note that the 2MASS AGN with far-IR measurements are at the tail of distribution — i.e., just those with IRAS detections — and their IR SEDs are not necessarily representative of 2MASS AGN in general.

5.3 Equivalent Width Distributions

Figure 12 shows $b_J - K_s$ color as a function of EW of the broad (permitted) emission line, Hβ, and the narrow (forbidden) emission line, [OIII] ($\lambda\,5008\,\text{Å}$). Traditionally, the broad emission lines are thought to originate from photoionized gas close to the central AGN known as the broad line region (BLR). The narrow lines from much further out, to a few hundred parsecs or more, are known as the narrow line region (NLR).

Overall, the Hβ and [OIII] EW distributions for our type I AGN are consistent with those of optically selected quasars (e.g., from SDSS). However, there is a clear separation in these EWs between our type I and II AGN and this is consistent with the AGN unified model. The Hβ line in most of the type II AGN appears intrinsically weaker than in type I AGN. This is because fewer ionizing photons are reaching and being reprocessed by the NLR due to, e.g., absorption and scattering by dust. In type I AGN, we have a direct view of the BLR line emission. Emission from the NLR can also contribute to the observed Hβ line flux in type I AGN. The type II AGN also appear to be redder on average in $b_J - K_s$ than the type I AGN. This is also consistent with the unified model if the continuum

flux in type II AGN suffers more extinction from dust, or if obscuration of the central AGN allows us to see more contribution from a 'redder' host galaxy, e.g., from old stellar populations.

The behavior in the EW of the narrow [OIII] emission line (Figure 12b) for type I and II AGN is reversed. Here, the [OIII] emission from type I AGN is reduced relative to the optical continuum because the latter is stronger (e.g., less extincted by dust) than that in type II AGN. This is consistent with the difference in $b_J - K_s$ color between the type I and II AGN being due to dust redenning. Interestingly, $b_J - K_s$ color is weakly but significantly correlated with [OIII] EW for each of the type I and type II classes. Pearson's product-moment correlation coefficient is 0.29 and 0.32 for the type I and type II AGN, respectively, with probabilities of <0.1% and <0.8% of these measures occuring by chance. Similar results are obtained using Kendall's non-parametric τ test.

These results suggest anisotropic obscuration of the central AGN and BLR, and that the bulk of the narrow-line emission originates from beyond the obscuring material. The type II AGN in particular require contamination by non-AGN light (e.g., galaxy hosts) if the AGN continuum source is obscured. Otherwise their [OIII] EWs will be much larger than observed. Scattered AGN light cannot account for the additional continuum since it is expected to be less than a few percent in these objects (Kuraszkiewicz et al. 2009). In addition, the overlap in EWs between our type I AGN and optically selected QSOs implies host-galaxy contamination of their optical continuum emission is minimal.

6 Conclusions

We have extended the 2MASS red AGN search to the southern equatorial sky and increased the statistical base of red AGN by $\simeq 35\%$ relative to previous surveys (primarily Cutri et al. 2002). We used the unique capabilities of the 6dF instrument and efficient observing strategy of

the 6dF Galaxy Redshift Survey to acquire spectra for 1182 candidates selected from the 2MASS PSC. Our main conclusions are

1. Classifications were secured for 432 spectra, of which 116 were securely identified as type I AGN with broad permitted emission lines exceeding $1000\,\mathrm{km\,s^{-1}}$ (FWHM). 57 were identified as type II AGN, all of which are tentative due to the non-spectrophotometric nature of their spectra, availability of appropriate emission line pairs, and line flux measurement uncertainties.

2. A majority of the type I AGN are new, with only eight ($\sim$6%) previously identified as AGN or QSOs in the literature. Most of them were previously classified as galaxy-like and extended in the optical (Super-COSMOS digitized plates) or near-IR (2MASS Atlas Images). 95% span the redshift range $0.05 < z < 0.5$.

3. Our selection method finds a significantly higher fraction of local galaxies containing AGN than in previous blue-selected galaxy surveys. Our red ($J - K_s \gtrsim 2$) color cut selects more AGN against the intrinsically blue galaxy light. We find that $\simeq$24% of our objects at $z < 0.05$ are associated with an AGN. For comparison, blue-selected galaxy samples are finding $\simeq$4%.

4. Comparing our ratio of type I to type II AGN to that found in previous studies of 2MASS red AGN, there is tentative evidence that this ratio increases with a redder $J - K_s$ color cut. This is consistent with the observation that most type II AGN have their optical-to-near-IR emission dominated by blue galaxy light, and that a redder $J - K_s$ cut will select more sources where the active nuclear emission dominates, i.e., type I AGN.

5. The optical colors of the 2MASS AGN constrain any extinction by dust at $A_V < 2$ mag relative to the SEDs of blue optically-selected QSOs. Most of the type I AGN are too blue in their optical colors for dust to significantly affect their optical/near-IR continua. There are also a handful of red type I AGN (with $b_J - K_s \gtrsim 4.5$) showing excess far-IR emission at $\lambda \gtrsim 80\,\mu\mathrm{m}$, and some at $50\,\mu\mathrm{m} < \lambda < 60\,\mu\mathrm{m}$. This suggests at least some 2MASS AGN reside in dusty environments.

6. The distribution of Hβ and [OIII] EWs, and optical/near-IR colors for type I and II AGN, are consistent with AGN unified models. The EW of the [OIII] emission line correlates with $b_J - K_s$ color in both types of AGN, suggesting anisotropic obscuration of the central AGN. The type II AGN require a significant contribution to their optical continua by stellar light to satisfy the EW measurements.

7. Overall, the optical properties of the 2MASS red AGN are not dramatically different from those found in optical QSO samples. This is most likely due to the relatively bright optical magnitude limit imposed for reliable spectroscopic identification. It appears that red AGN selection in 2MASS detects the most luminous objects in the near-IR in the local universe to $z \simeq 0.6$. This is an impetus to use similar methods for future deep near-IR surveys. Indeed, such surveys have already begun to unravel a new population of AGN at high redshift.

References

Baldwin, J. A., Phillips, M. M. & Terlevich, R., 1981, PASP, 93, 5

Barkhouse, W. A. & Hall, P. B., 2001, AJ, 121, 2843

Benn, C. R., Vigotti, M., Carballo, R., Gonzalez-Serrano, J. I. & Sánchez, S. F., 1998, MNRAS, 295, 451

Blair, M. & Gilmore, G., 1982, PASP, 94, 742

Brown, M. J. I. et al., 2006, ApJ, 638, 88

Colless, M. et al., 2001, MNRAS, 328, 1039

Croom, S. M., Warren, S. J. & Glazebrook, K., 2001, MNRAS, 328, 150

Cutri, R. M., Nelson, B. O., Francis, P. J. & Smith, P. S., 2002, in Proc. ASP Conf. 284, Eds. Green, R. F., Khachikian, E. Ye. & Sanders, D. B., 127

Desroches, L.-B. & Ho, L., 2009, ApJ, 690, 267

Donley, J. L., Rieke, G. H., Pérez-González, P. G. & Barro, G., 2008, ApJ, 687, 111

Elvis, M., Wilkes, B. J., McDowell, J. C., Green, R. F., Bechtold, J., Willner, S. P., Oey, M. S., Polomski, E. & Cutri, R., 1994, ApJs, 95, 1

Francis, P. J., Whiting, M. T. & Webster, R. L., 2000, PASA, 17, 56

Francis, P. J., Nelson, B. O. & Cutri, R. M., 2004, AJ, 127, 646

Fraquelli, H. A. & Storchi-Bergmann, T., 2004, in Proc. IAU Symp. 222, Eds. Storchi-Bergmann, T., Ho, L. C. & Schmitt, H. R. (Cambridge, UK: Cambridge University Press), 319

Fukugita, M., Shimasaku, K. & Ichikawa, T., 1995, PASP, 107, 945

Georgakakis, A., Clements, D. L., Bendo, G., Rowan-Robinson, M., Nandra, K. & Brotherton, M. S., 2009, MNRAS, 394, 533

Glikman, E., Gregg, M. D., Lacy, M., Helfand, D. J., Becker, R. H. & White, R. L., 2004, ApJ, 607, 60

Glikman, E., Helfand, D. J., White, R. L. & Becker, R. H., 2007, ApJ, 667, 673

Gregg, M. D., Lacy, M., White, R. L., Glikman, E., Helfand, D., Becker, R. H. & Brotherton, M. S., 2002, ApJ, 564, 133

Hambly, N. C. et al., 2001a, MNRAS, 326, 1279

Hambly, N. C. et al., 2001b, MNRAS, 326, 1295

Hao, L. & Strauss, M. A., 2004, Carnegie Observatories Astrophysics Series, Vol. 1., Coevolution of Black Holes and Galaxies (Cambridge, UK: Cambridge University Press) 23

Hewett, P. C., Foltz, C. B. & Chaffee, F. H., 1995, AJ, 109, 1498

Ho, L. C., Filippenko, A. V. & Sargent, W. L. W., 1997, ApJs, 112, 315

Ho, L. C. (Ed.), 2004, Carnegie Observatories Astrophysics Series, Vol. 1., Coevolution of Black Holes and Galaxies (Cambridge, UK: Cambridge University Press)

Huber, P. J., 1981, Wiley Series in Probability and Mathematical Statistics (New York: Wiley)

Huchra, J. & Burg, R., 1992, ApJ, 393, 90

Jarrett, T. H., Chester, T., Cutri, R., Schneider, S., Skrutskie, M. & Huchra, J. P., 2000, AJ, 119, 2498

Jarrett, T. H., 2004, PASA, 21, 396

Jones, D. H. et al., 2004, MNRAS, 355, 747

Jones, D. H. et al., 2009, MNRAS, in press (arXiv:0903.5451)

Jurek, R. J., Drinkwater, M. J., Francis, P. J. & Pimbblet, K. A., 2008, MNRAS, 383, 673

Kewley, L. J., Heisler, C. A., Dopita, M. A. & Lumsden, S., 2001, ApJs, 132, 37

Kewley, L. J., Groves, B., Kauffmann, G. & Heckman, T., 2006, MNRAS, 372, 961

Kuraszkiewicz, J., Wilkes, B. J., Schmidt, G., Ghosh, H., Smith, P. S., Cutri, R., Hines, D., Huff, E. M., McDowell, J. C. & Nelson, B., 2009, ApJ, 692, 1143

Low, F. J., Cutri, R. M., Huchra, J. P. & Kleinmann, S. G., 1988, ApJ, 327, L41

Maddox, N., Hewett, P. C., Warren, S. J. & Croom, S. M., 2008, MNRAS, 386, 1605

Masci, F. J., Webster, R. L. & Francis, P. J., 1998, MNRAS, 301, 975

Moultaka, J., Ilovaisky, S. A., Prugniel, P. & Soubiran, C., 2004, PASP, 116, 693

Polletta, M. et al., 2007, ApJ, 663, 81

Richards, G. T. et al., 2002, AJ, 123, 2945

Richards, G. T. et al., 2003, AJ, 126, 1131

Sanders, D. B., Phinney, E. S., Neugebauer, G., Soifer, B. T. & Matthews, K., 1989, ApJ, 347, 29

Saunders, W. et al., 2001, Anglo-Australian Observatory Newsletter, 97, 14

Schneider, D. P. et al., 2007, AJ, 134, 102

Schlegel, D. J., Finkbeiner, D. P. & Davis, M., 1998, ApJ, 500, 525

Schmidt, M. & Green, R. F., 1983, ApJ, 269, 352

Sharp, R. G., Sabbey, C. N., Vivas, A. K., Oemler, A., McMahon, R. G., Hodgkin, S. T. & Coppi, P. S., 2002, MNRAS, 337, 1153

Skrutskie, M. F. et al., 2006, AJ, 131, 1163

Smail, I., Sharp, R., Swinbank, A. M., Akiyama, M., Ueda, Y., Foucaud, S., Almaini, O. & Croom, S., 2008, MNRAS, 389, 407

Smith, P. S., Schmidt, G. D., Hines, D. C., Cutri, R. M. & Nelson, B. O., 2002, ApJ, 569, 23

Spinoglio, L. & Malkan, M. A., 1989, ApJ, 342, 83

Vanden Berk, D. E. et al., 2001, AJ, 122, 549

Veron-Cetty, M. P. & Veron, P., 2000, ESO Sci. Rep., 19, 1

Warren, S. J., Hewett, P. C. & Foltz, C. B., 2000, MNRAS, 312, 827

Watson, F. G., Parker, Q. A. & Miziarski, S., 1998, SPIE, 3355, 834

Webster, R. L., Francis, P. J., Peterson, B. A., Drinkwater, M. J. & Masci, F. J., 1995, Nature, 375, 469

Wilkes, B. J., Schmidt, G. D., Cutri, R. M., Ghosh, H., Hines, D. C., Nelson, B. & Smith, P. S., 2002, ApJ, 564, L65

Zakamska, N. L. et al., 2003, AJ, 126, 2125